NKp46 Receptor-Mediated Interferon-γ Production by Natural Killer Cells Increases Fibronectin 1 to Alter Tumor Architecture and Control Metastasis

Glasner, Ariella; Levi, Assi; ...; Jonjić, Stipan; ...; Mandelboim, Ofer

Source / Izvornik: **Immunity, 2018, 48, 107 - 119**

Journal article, Published version
Rad u časopisu, Objavljena verzija rada (izdavačev PDF)

https://doi.org/10.1016/j.immuni.2017.12.007

Permanent link / Trajna poveznica: https://urn.nsk.hr/urn:nbn:hr:184:184731

Article

Immunity

NKp46 Receptor-Mediated Interferon-γ Production by Natural Killer Cells Increases Fibronectin 1 to Alter Tumor Architecture and Control Metastasis

Graphical Abstract

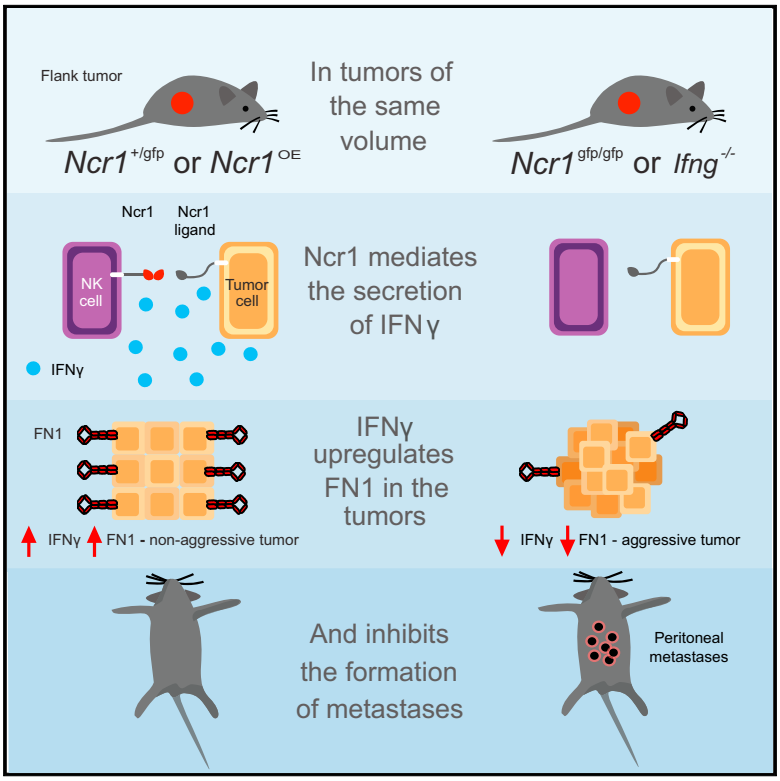

Highlights

- NKp46 expression on NK cells controls growth of melanoma and carcinoma metastases
- In the absence of NKp46, tumor architectural properties indicate an aggressive phenotype
- NK cell NKp46-mediated IFN-γ production controls tumor structure via FN1 induction
- IFN-γ treatment or Ncr1 overexpression in tumor-bearing mice decreases tumor metastases

Authors

Ariella Glasner, Assi Levi, Jonatan Enk, ..., Barbara Seliger, Laurence Zitvogel, Ofer Mandelboim

Correspondence

oferm@ekmd.huji.ac.il

In Brief

NK cells defend against various pathogens and tumors, but the mechanisms by which they control tumor metastases are not clear. Here, Glasner et al. show that NK cells prevent tumor metastases *in vivo* by editing tumor architecture via NKp46-mediated IFN-γ production that leads to upregulation of extracellular matrix protein FN1 in the tumor.

Glasner et al., 2018, Immunity *48*, 107–119
January 16, 2018
https://doi.org/10.1016/j.immuni.2017.12.007

CellPress

Immunity
Article

NKp46 Receptor-Mediated Interferon-γ Production by Natural Killer Cells Increases Fibronectin 1 to Alter Tumor Architecture and Control Metastasis

Ariella Glasner,[1,12] Assi Levi,[2,12] Jonatan Enk,[1] Batya Isaacson,[1] Sergey Viukov,[3] Shari Orlanski,[4] Alon Scope,[5] Tzahi Neuman,[6] Claes D. Enk,[7] Jacob H. Hanna,[3] Veronika Sexl,[8] Stipan Jonjic,[9] Barbara Seliger,[10] Laurence Zitvogel,[11] and Ofer Mandelboim[1,13,*]

[1]The Lautenberg Center for General and Tumor Immunology, Department of Immunology and Cancer Research, IMRIC, Faculty of Medicine, The Hebrew University Medical School, Jerusalem, Israel
[2]Photodermatosis Clinic, Department of Dermatology, Rabin Medical Center, Petah-Tikva, Israel and Sackler Faculty of Medicine, Tel Aviv University, Tel Aviv, Israel
[3]Department of Molecular Genetics, Weizmann Institute of Science, Rehovot 7610001, Israel
[4]Department of Developmental Biology and Cancer Research, Institute for Medical Research Israel-Canada, Hebrew University Medical School, Jerusalem, Israel
[5]Medical Screening Institute, Sheba Medical Center and Sackler School of Medicine, Tel Aviv University, Tel Aviv, Israel
[6]Department of Pathology, Hadassah Medical Organization, The Hebrew University Medical Center, Jerusalem, Israel
[7]Department of Dermatology, Hadassah-Hebrew University Medical School, Jerusalem, Israel
[8]Institute of Pharmacology and Toxicology, University of Veterinary Medicine, Vienna, Austria
[9]Department of Histology and Embryology Center for Proteomics, Faculty of Medicine, University of Rijeka, B. Branchetta, Rijeka, Croatia
[10]Institute of Medical Immunology, Martin Luther University Halle-Wittenberg, 06112 Halle, Germany
[11]Center of Clinical Investigations and U1015 INSERM, Gustave Roussy Cancer Campus, University Paris Saclay, Villejuif-Grand-Paris, France
[12]These authors contributed equally
[13]Lead Contact
*Correspondence: oferm@ekmd.huji.ac.il
https://doi.org/10.1016/j.immuni.2017.12.007

SUMMARY

Natural killer (NK) cells are innate lymphoid cells, and their presence within human tumors correlates with better prognosis. However, the mechanisms by which NK cells control tumors *in vivo* are unclear. Here, we used reflectance confocal microscopy (RCM) imaging in humans and in mice to visualize tumor architecture *in vivo*. We demonstrated that signaling via the NK cell receptor NKp46 (human) and Ncr1 (mouse) induced interferon-γ (IFN-γ) secretion from intratumoral NK cells. NKp46- and Ncr1-mediated IFN-γ production led to the increased expression of the extracellular matrix protein fibronectin 1 (FN1) in the tumors, which altered primary tumor architecture and resulted in decreased metastases formation. Injection of IFN-γ into tumor-bearing mice or transgenic overexpression of Ncr1 in NK cells in mice resulted in decreased metastasis formation. Thus, we have defined a mechanism of NK cell-mediated control of metastases *in vivo* that may help develop NK cell-dependent cancer therapies.

INTRODUCTION

NK cells are cytotoxic innate lymphoid cells (ILCs), which kill malignant cells (Elboim et al., 2010; Glasner et al., 2012a; Halfteck et al., 2009; Koch et al., 2013; Morvan and Lanier, 2016), virus-infected cells (Bar-On et al., 2013, 2014; Diab et al., 2016, 2017; Gazit et al., 2006; Glasner et al., 2012b, 2015a; Seidel et al., 2012), bacteria (Chaushu et al., 2012; Gur et al., 2013a, 2015), and fungi (Vitenshtein et al., 2016) and also play a role in autoimmunity (Gur et al., 2010, 2011, 2012, 2013b; Wensveen et al., 2015), allergy (Ghadially et al., 2013), and graft-versus-host disease (Ghadially et al., 2014). NK cell killing is executed following engagement of activating receptors, which include, among others, the natural cytotoxicity receptors (NCRs) NKp30, NKp44, and NKp46 (Ncr1 in mice). Triggering of NKp46 leads not only to perforin-mediated direct cytotoxicity, but also to secretion of inflammatory cytokines, mainly IFN-γ and TNF-α (Morvan and Lanier, 2016).

Several pathogen-derived ligands have been identified for NKp46 such as the influenza, Sendai, and Newcastle disease hemaglutinins (HAs) (Draghi et al., 2007; Gazit et al., 2006; Jarahian et al., 2009, 2011; Mandelboim et al., 2001), but the identities of its membrane-bound cellular and tumor ligands remain largely unknown. To study NKp46 and Ncr1 activity *in vivo*, we generated an Ncr1 knockout (KO) mouse in which *Ncr1* was replaced by a green fluorescent protein (GFP) reporter ($Ncr1^{gfp/gfp}$) (Gazit et al., 2006). In the heterozygous $Ncr1^{+/gfp}$ mice (which are immune competent, as one Ncr1 allele is still present) and in the *Ncr1*-deficient mice, NK cells develop normally (Gazit et al., 2006; Glasner et al., 2015b; Satoh-Takayama et al., 2009; Sheppard et al., 2013). Using these mice, we have demonstrated that Ncr1 is involved in tumor elimination. Specifically, Ncr1 was shown to control the growth of melanoma (Lakshmikanth et al., 2009), lymphoma (Halfteck

et al., 2009), carcinoma (Glasner et al., 2012a), and carcinogen-induced fibrosarcoma (MCA) (Elboim et al., 2010). However, the mechanisms by which NK cells control tumor development and metastases via Ncr1, *in vivo*, remain largely unknown.

NK cell control of tumor metastases is especially intriguing, as the presence of NK cells within tumors is usually sparse (Delahaye et al., 2011; Desbois et al., 2012). However, in their absence, increased tumor growth and metastasis were described (Morvan and Lanier, 2016) and the numbers of NK cells in tumors correlates with better prognosis and less likelihood to develop metastases (Delahaye et al., 2011).

Melanoma is a potentially deadly cutaneous malignancy. Although its prevalence is much lower compared to other skin neoplasms such as basal cell carcinoma and squamous cell carcinoma, it remains the leading cause of death from skin cancers (Guy and Ekwueme, 2011). Although recent development in the treatment of advanced-stage melanoma yielded substantial improvement in survival (Breunis et al., 2008; Flaherty et al., 2010; Parakh et al., 2017), disease prevention mainly by avoidance of solar damage is still advocated. Yet in spite of increased use of topical ultraviolet (UV) filters, melanoma incidence is constantly on the rise (Arnold et al., 2014). Therefore, early diagnosis and rapid surgical removal of the tumors are critical.

Reflectance confocal microscopy (RCM) is a novel, non-invasive imaging technique that permits real-time visualization of cellular components in the skin at a resolution close to that of conventional histology. A detailed description of RCM methodology is available in the STAR Methods. Here we employed RCM imaging in humans and various mouse models to study the role of NKp46 and Ncr1 in controlling tumors and metastases *in vivo*. We found that triggering of Ncr1 led to IFN-γ secretion which in turn led to increased fibronectin1 (FN1) expression in the tumors, affecting their structure and resulting in decreased metastases.

RESULTS

NK Cells Control B16 Tumors and Metastases in an Ncr1-Dependent Manner

NKp46 (Ncr1 in mice) is a major NK cell receptor, whose expression is almost exclusive to NK cells (Delahaye et al., 2011; Desbois et al., 2012; Morvan and Lanier, 2016). In our previous studies, we observed that although Ncr1 does not affect the development of primary tumors growing in the footpad, it does control the formation of lung metastases (Glasner et al., 2012a). However, the mechanisms responsible for these effects are unknown. To investigate whether NK cells, via Ncr1, can control primary tumor growth in additional locations (other than the footpad), we inoculated 1×10^6 B16F10.9 melanoma (B16) cells subcutaneously (s.c.) into the flank of $Ncr1^{+/gfp}$ and $Ncr1^{gfp/gfp}$ mice. In accordance with our previous findings (Glasner et al., 2012a), no differences were observed in the flank B16 tumor growth rate between the various mice groups (Figure 1A). However, similarly to our previous results, almost half the $Ncr1^{gfp/gfp}$ mice developed spontaneous peritoneal metastases, compared to only about 10% in the immune-competent $Ncr1^{+/gfp}$ mice (Figure 1B). We next injected 10-fold decreasing doses of tumor cells directly into the peritoneum to generate experimental peritoneal metastases. However, even in the lowest cell dose, no difference was observed in the Ncr1 ability to control B16 metastases (Figure 1C, the graph represents mortality rate following metastases formation). This led us to conclude that Ncr1 affects metastases formation irrespective of the primary tumor development, not by restricting tumor growth, but by other mechanisms.

Tumor Properties Are Similar in the Presence or Absence of Ncr1

To test whether the developing tumors change the expression of their unknown Ncr1 ligand following the Ncr1-mediated immune pressure, we isolated primary tumors that had developed in $Ncr1^{+/gfp}$ and in $Ncr1^{gfp/gfp}$ mice. As the membrane-bound tumor ligand (or ligands) for Ncr1 and NKp46 are unknown, we stained the tumor cell lines with Ncr1 Ig fusion proteins and observed no differences (Figure 1D). Similarly, biochemical properties of the unknown Ncr1 tumor ligand were identical in the presence or absence of Ncr1, being insensitive to neuraminidase (NA) and sensitive to trypsin and proteinase K (Figure 1E). A CD107a mobilization assay confirmed that all tumors elicited reduced degranulation in the absence of Ncr1, regardless of the tumor origin (Figure 1F). We also observed similar levels of transcripts associated with immune cell populations, such as NK cells (Figure 1G) and other immune cells (Figures 1H–1L) within the $Ncr1^{+/gfp}$ and $Ncr1^{gfp/gfp}$ mice tumors. Therefore, we concluded that primary B16 melanoma tumors develop similarly in the presence and absence of Ncr1 and that Ncr1 controls B16 metastases.

Ncr1 Control of Metastatic Activity Is Mediated by IFN-γ

To test whether the absence of Ncr1 would affect cytokine secretion, we incubated B16 cells with NK cells isolated from the $Ncr1^{+/gfp}$ and $Ncr1^{gfp/gfp}$ mice for 12 hr. IFN-γ and TNFα production (pg/mL) by $Ncr1^{+/gfp}$ NK cells was higher compared to $Ncr1^{gfp/gfp}$ NK cells (Figure 1M). B16 cells express the IFN-γ receptor (IFN-γR) but lack expression of the TNFα receptor (TNFαR) (Figure 1N), suggesting that IFN-γ but not TNFα affect B16 tumor development and metastases. To demonstrate the direct Ncr1 involvement in IFN-γ secretion, we incubated $Ncr1^{+/gfp}$ and $Ncr1^{gfp/gfp}$ NK cells with B16 targets in the absence or in the presence of a blocking anti-Ncr1 antibody. IFN-γ secretion was similar in the absence of Ncr1 ($Ncr1^{gfp/gfp}$) and following Ncr1 blocking (Figure 1O), indicating that the observed effect is mediated directly by Ncr1.

We next injected B16 tumors into $Ncr1^{+/gfp}$ and $Ncr1^{gfp/gfp}$ mice as above, as well as into IFN-γ-deficient ($Ifng^{-/-}$) and TNFα-deficient ($Tnfa^{-/-}$) mice. While primary B16 tumor growth was similar in all mice (Figure 1P), more metastases were observed in the $Ifng^{-/-}$ and $Ncr1^{gfp/gfp}$ mice (Figure 1Q). These findings suggest that NK cells' ability to control metastases is mediated by IFN-γ.

Human Melanomas Exhibited Aggressive Structural Properties Compared to Nevi, as Revealed by RCM Imaging

To investigate how Ncr1, via the secretion of IFN-γ, modulates the primary tumors and prevents metastases, we employed RCM imaging. First, we imaged human melanomas and nevi.

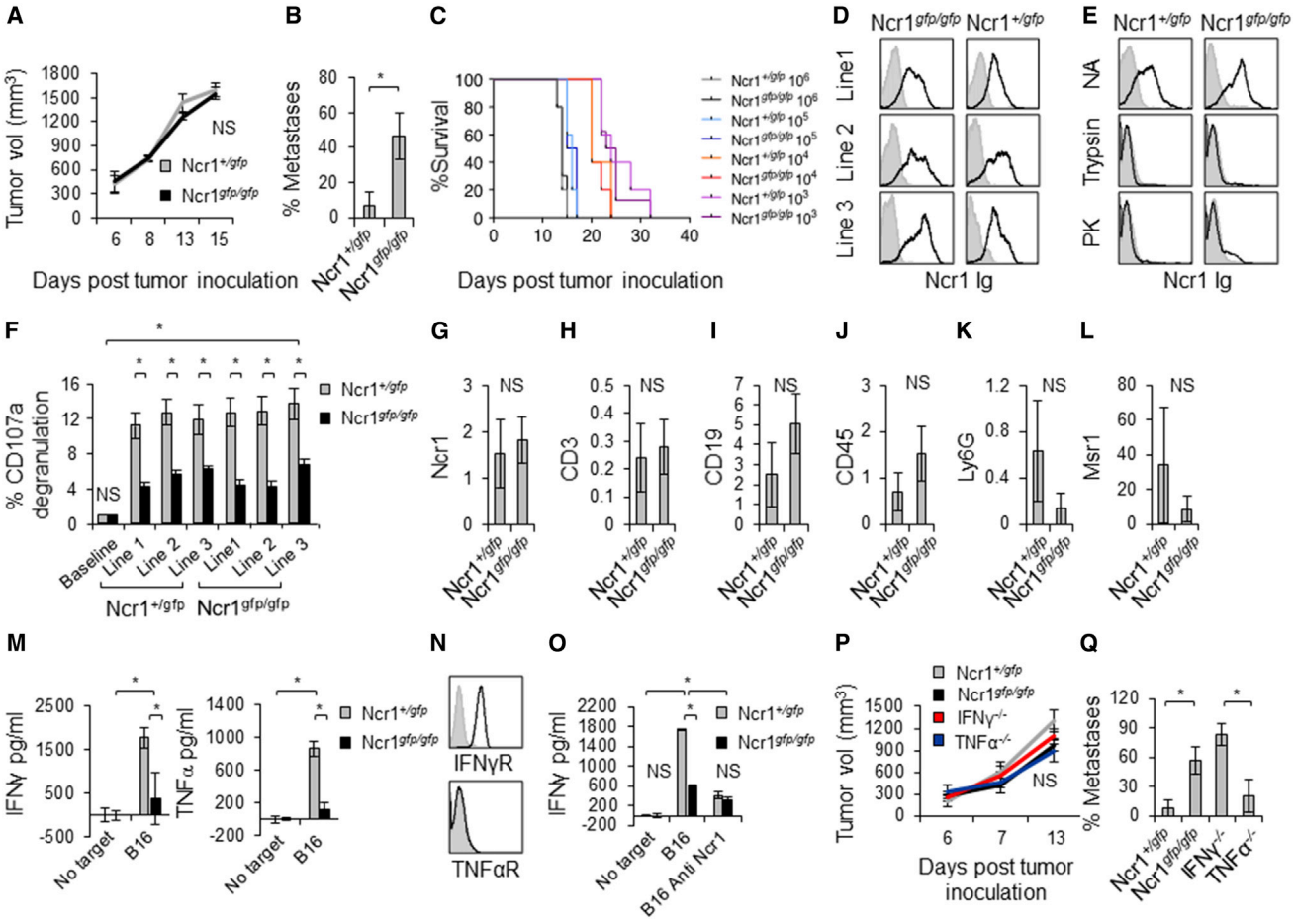

Figure 1. Ncr1 Controls B16 Metastases

(A) Tumor volume after s.c. inoculation of 1 × 10^6 B16 cells.

(B) Spontaneous metastasis in the same animals presented in (A).

(C) Mice survival after intraperitoneal growth of B16 metastases.

(D and E) FACS staining of B16 cell lines obtained from the tumors originated in *Ncr1*$^{+/gfp}$ or *Ncr1*$^{gfp/gfp}$ mice with Ncr1 Ig. Tumors were untreated (D) or treated with the indicated proteases (E). For (D) and (E), black line histograms represent specific staining. Gray filled histograms are secondary mAb background control of the untreated cells. Each FACS plot is representative of at least three independent experiments.

(F) CD107a degranulation following 2-hr incubation of B16 cells that developed in *Ncr1*$^{+/gfp}$ or *Ncr1*$^{gfp/gfp}$ mice with poly(I:C)-activated NK cells obtained from *Ncr1*$^{+/gfp}$ and the *Ncr1*$^{gfp/gfp}$ mice. Ten mice were used in each group. The experiment was repeated three times. Values are shown as mean ± SEM. *$p < 0.05$.

(G–L) qRT-PCR presenting relative expression of various immune cell markers in B16 tumors. qRT-PCR assays were performed on triplicates, normalized to GAPDH and ACTB. Each experiment was repeated three times. Values are shown as mean ± SEM. *$p < 0.05$. NS, non-significant. In (G), NK cells were detected using primers targeting exons 1–4 of Ncr1 as in the *Ncr1*$^{gfp/gfp}$ mice exons 5–7 of Ncr1 were replaced by gfp, whereas exons 1–4 are still present.

(M) IFN-γ and TNFα secretion by NK cells derived from *Ncr1*$^{+/gfp}$ or *Ncr1*$^{gfp/gfp}$ mice following incubation with B16 cells.

(N) FACS staining of B16 cells. Black line histograms represent specific staining. Gray filled histograms represent background control.

(O) IFN-γ secretion by NK cells derived from *Ncr1*$^{+/gfp}$ or *Ncr1*$^{gfp/gfp}$ mice following incubation with B16 cells, in the presence or absence of a blocking Ncr1 antibody.

(P) Tumor volume following s.c. flank inoculation of 1 × 10^6 B16 cells.

(Q) Spontaneous metastasis in the animals presented in (P). At least eight mice were used in each group.

Values are shown as mean ± SEM. *$p < 0.05$. NS, non-significant

Figure S1 shows two human skin lesions that appear similar to the naked eye (Figures S1A and S1J). However, RCM evaluation, based on tissue architecture parameters (Pellacani et al., 2007), enabled the accurate classification of the two lesions as nevus (Figures S1A–S1I) and melanoma (Figures S1J–S1R). A detailed description of the analysis is provided in the STAR Methods. We used RCM to evaluate tissue architecture in 11 human melanomas compared to 5 nevi and detected significant differences in all RCM criteria (summarized in Figures S1S–S1Z). Thus, RCM can be used to distinguish between human melanomas and nevi.

Only very few works employ RCM in mice (Chernyavskiy et al., 2009; Li et al., 2005; Park et al., 2010). To test whether mouse melanoma tumors would present RCM features similarly to human melanomas, we performed RCM on B16 tumors and observed that all human melanoma RCM criteria were also

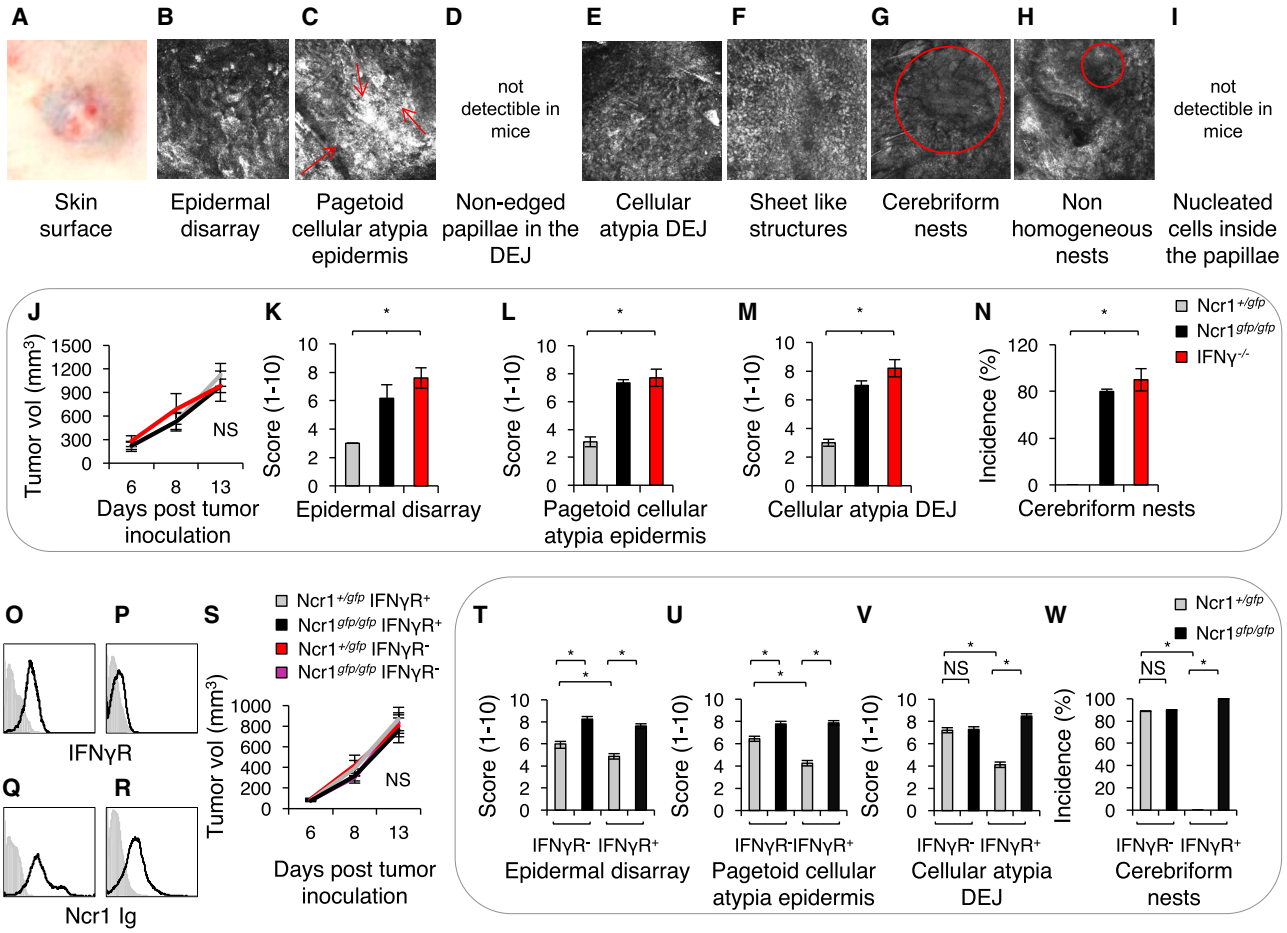

Figure 2. Ncr1 Edits B16 Structure via IFN-γ

(A) An *in vivo* photo of a B16 tumor taken at time of RCM.

(B–I) *In vivo* RCM images of B16 tumors.

(J) Tumor volume at time of RCM following s.c. inoculation of 1 × 10^6 B16 cells.

(K–N) Quantification of the RCM features (described in the STAR Methods) assessed on the tumors presented in (J). Scoring: 1 = least aggressive to 10 = most aggressive.

(O–R) FACS staining of B16 lines used in (S)–(W). Black line indicates specific staining; gray filled histogram indicates background control.

(S) Tumor volume following s.c. inoculation of 1 × 10^6 B16 cells.

(T–W) Quantification of RCM features.

For (J)–(N) and (S)–(W), at least eight mice were used in each group. Values are shown as mean ± SEM. *$p < 0.05$, NS, non-significant. See also Figures S1 and S2.

detectable in the B16 mouse tumors (Figures 2A–2I) except non-edged papillae (Figure 2D) and nucleated cells inside the papillae (Figure 2I). This is likely because the basal layer is very thin in mice and dermal papillae are hard to demonstrate. These findings confirmed RCM as a reliable method to characterize the structural properties of mouse tumors and that B16 melanomas are structurally similar to human melanomas.

Ncr1, via IFN-γ Secretion, Modulates the Structural Features of B16 Primary Tumors

To image tumor architecture *in vivo*, in the absence of Ncr1 and IFN-γ, we inoculated *Ncr1*$^{+/gfp}$, *Ncr1*$^{gfp/gfp}$, and *Ifng*$^{-/-}$ mice with 1 × 10^6 B16 cells and monitored tumor growth. RCM was performed on tumors of the same volume at two time points: around 1 week and around 2 weeks after tumor inoculation (Figure 2J). RCM analysis revealed significantly worse structural properties for tumors that developed in *Ncr1*$^{gfp/gfp}$ and *Ifng*$^{-/-}$ mice according to four RCM criteria (Figures 2K–2N). These criteria have been previously shown, in humans, to correlate with metastatic activity (Pellacani et al., 2007; Wisco and Sober, 2012). As these differences were detected at both time points (Figures 2K–2N show only the early time point), RCM evaluation was performed around 1 week after tumor inoculation henceforth. No differences were observed in two other RCM features (sheet-like structures and non-homogeneous nests, data not shown). To corroborate these findings, we evaluated *Ncr1*$^{+/gfp}$ and *Ncr1*$^{gfp/gfp}$ B16 tumors by conventional histology, using hematoxylin and eosin (H&E) staining. As seen in Figure S2, and in agreement with the results observed using RCM, worse structural properties were detected for *Ncr1*$^{gfp/gfp}$ B16 tumors

compared to *Ncr1*$^{+/gfp}$ tumors. (Figure S2A depicts epidermal invasiveness, quantified in Figure S2B; Figure S2C depicts ulceration, quantified in Figure S2D; Figure S2E depicts muscle invasiveness, quantified in Figure S2F; and Figure S2G depicts lung metastases, quantified in Figure S2H. Figure S2I shows lower-magnification images of a whole lung lobe for better clarity.)

To test whether IFN-γ secretion alters the structural features of the B16 tumors directly, we isolated B16 clones expressing IFN-γR (Figure 2O) or not (Figure 2P). After having verified similar expression of the unknown Ncr1 ligand (Figures 2Q and 2R), we injected the tumors into the flanks of *Ncr1*$^{+/gfp}$ and *Ncr1*$^{gfp/gfp}$ mice. Again, RCM was performed on tumors of the same volume and developmental stage (Figure 2S). In the absence of IFN-γR, differences in the four RCM criteria between the groups were significantly diminished or completely abolished (Figures 2T–2W). Therefore, we concluded that Ncr1-mediated IFN-γ is at least partially responsible for editing the tumor structural properties and that IFN-γ acts directly on the tumor cells to modulate tumor architecture.

IFN-γ Secretion Upregulates FN1, Resulting in a Structural Organization that Restricts Metastases Formation

To determine the mechanisms by which Ncr1 edits tumor structure via IFN-γ, we performed RNA sequencing (RNA-seq) on biological triplicates of IFN-γ-treated and untreated B16 cells. Around 7,000 genes were differentially expressed. As expected, the vast majority of the differentially expressed genes coded for proteins participating in antiviral defense, immune response, and MHC regulation (examples are shown in Figure S3A). As we observed that Ncr1 affects tumor architecture, we searched for changes in the expression of structural genes, cell adhesion, and cellular matrix proteins (Figure S3A). Among the enriched structural genes, the expression of the extracellular matrix protein fibronectin1 (FN1) was increased by 24-fold (Figures 3A, S3A, and S3B). This finding was validated in the presence or absence of IFN-γ, using western blotting (WB) (Figure 3B) and quantitative reverse transcription polymerase chain reaction (qRT-PCR) (Figure 3C).

To demonstrate the effect FN1 has on tumor architecture, we initially tried to overexpress FN1 in B16 and other tumors, using various methods without success, probably due to its high molecular weight (~440 kDa). Instead, we knocked down (KD) FN1 in B16 cells using five independent short hairpin RNA (shRNAs). Figures 3D (WB) and 3E (qRT-PCR) represent one KD line. Figure S4A shows all control and KD lines generated. We then inoculated *Ncr1*$^{+/gfp}$, *Ncr1*$^{gfp/gfp}$, and *Ifng*$^{-/-}$ mice with the control and FN1 KD B16 cells and monitored tumor growth. As before, all tumors developed with comparable kinetics (Figure 3F). Mice inoculated with FN1 KD melanomas exhibited increased metastasis (Figure 3G). Furthermore, all mice injected with the FN1 KD tumors showed worse RCM scores (Figures 3H–3K, one representative KD line; and Figures S4B–S4E, all KD and control lines generated).

To demonstrate that FN1 is expressed *in vivo* in an Ncr1-dependent manner, we harvested the B16 tumors from *Ncr1*$^{+/gfp}$, *Ncr1*$^{gfp/gfp}$, and *Ifng* $^{-/-}$ mice and performed FN1 immunofluorescence (IF) staining. The expression of FN1 in tumors obtained from *Ncr1*$^{gfp/gfp}$ and *Ifng* $^{-/-}$ mice was significantly reduced, compared to the *Ncr1*$^{+/gfp}$ mice (Figure 3L, quantified in 3M [fluorescence intensity] and in 3N [qRT-PCR]). We concluded that IFN-γ mediated the elevated expression of FN1 in the tumors and that in the absence of IFN-γ or FN1, tumors were more aggressive.

Ncr1 Edits Lewis Lung Carcinoma Tumors via IFN-γ and FN1 and Prevents Metastases

To demonstrate that the Ncr1-dependent structural editing of tumors is not restricted to a particular cell line or tumor type, we next used the Lewis lung carcinoma line D122 (Eisenbach et al., 1983a; Glasner et al., 2012a). D122 tumors expressed IFN-γR (Figure 4A) and the unknown Ncr1 ligand (Figure 4B). D122 cells elicited significantly higher IFN-γ and TNFα secretion by NK cells derived from *Ncr1*$^{+/gfp}$ than *Ncr1*$^{gfp/gfp}$ mice (Figure S5A). The IFN-γ secretion was abolished in the presence of an Ncr1 blocking antibody (Figure S5B). Like B16, FN1 expression in D122 cells was significantly elevated following IFN-γ treatment (Figures 4C [WB] and 4D [qRT-PCR]). We generated control and five independent FN1 KD D122 lines (Figures 4E and 4F showing one representative KD line and Figure S5C showing all KD and control lines generated) and inoculated *Ncr1*$^{+/gfp}$, *Ncr1*$^{gfp/gfp}$, and *Ifng*$^{-/-}$ mice with a control or FN1 KD D122 tumors.

As the use of RCM imaging is restricted to skin neoplasms, the D122 tumors were inspected using conventional histopathology, which was performed on tumors of the same developmental stage and volume (Figure 4G). Worse structural properties such as ulceration (Figures 4H–4J), muscle invasiveness (Figures 4K–4M), and metastasis (Figures 4N–4P) were observed in the tumors grown in Ncr1- or in IFN-γ-deficient mice, as well as in all FN1 KD tumors, irrespective of mouse genotype. In line with these observations, FN1 expression was significantly reduced *in vivo* in the *Ncr1*$^{gfp/gfp}$ and *Ifng*$^{-/-}$ tumors and in all FN1 KD D122 tumors (Figure 4Q, one representative FN1 KD line is shown).

IFN-γ Treatment and Ncr1 Overexpression Prevent Metastases

Based on all of the above, we concluded that IFN-γ treatment should impair metastasis via FN1 induction. To test this, we injected B16-bearing mice with IFN-γ. Reduced metastases formation was observed in all IFN-γ-treated mice (Figure 5A), and RCM properties were significantly improved upon IFN-γ treatment, regardless of the mice genotype (Figures 5B–5E).

We also concluded that overexpressing Ncr1 in NK cells may offer a therapeutic opportunity to suppress metastasis. To test this, we used a transgenic mouse that we have generated (Glasner et al., 2017) in which Ncr1 is overexpressed specifically in NK cells (denoted Ncr1^{cre} Ncr1^{OE}). Inoculation of Ncr1^{cre} Ncr1^{OE} mice and littermate controls with B16 cells resulted in the comparable development of primary tumors (Figure 5F). However, fewer metastases developed in Ncr1^{cre} Ncr1^{OE} mice, compared to littermate controls (Figure 5G). RCM features were better in Ncr1^{cre} Ncr1^{OE} mice as well (Figures 5H–5K), paralleled by higher levels of Ncr1, IFN-γ, and FN1 (Figures 5L–5N).

Throughout the course of this study, we evaluated tumor volume and metastases in several independent experiments and in various different mouse groups. To account for

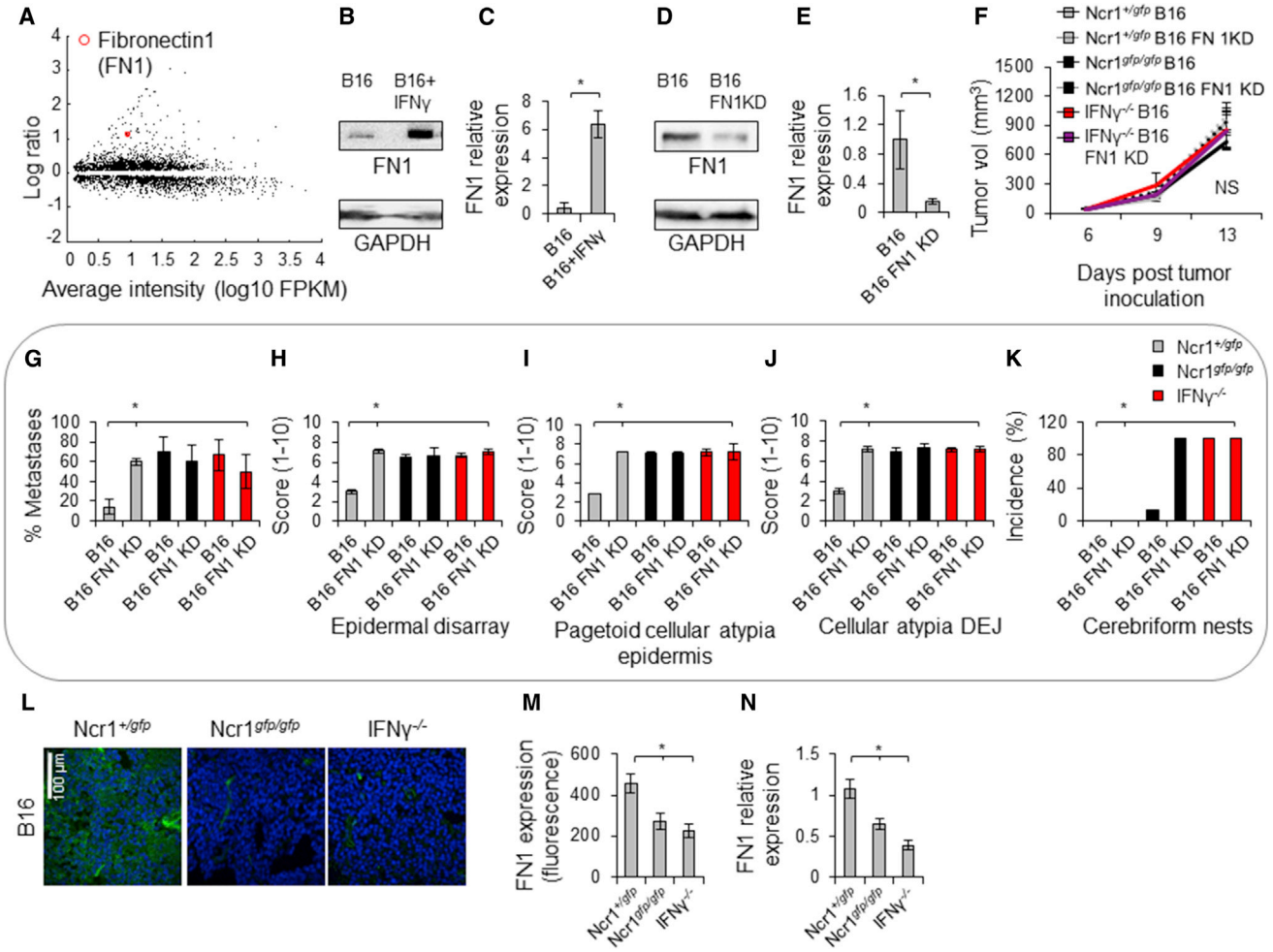

Figure 3. FN1 Mediates the Ncr1-Dependent Structural Editing of B16 Tumors

(A) Volcano plot of relative gene expression in B16 and IFN-γ-treated B16 cells, performed on biological triplicates.

(B and D) WB figures are representative of at least three experiments in each assay. Contrast was adjusted to facilitate visualization.

(C and E) qRT-PCR assays were performed on biological triplicates, normalized to GAPDH and ACTB. Each experiment was repeated three times. Values are shown as mean ± SEM.

(F) Tumors volume following s.c. inoculation of 1×10^6 B16 cells.

(G) Spontaneous metastasis in the animals presented in (F).

(H–K) Quantification of RCM features.

For (F)–(K), at least eight mice were used in each group. Values are shown as mean ± SEM.

(L) Representative IF staining for FN1, quantified in (M).

(N) qRT-PCR for FN1 in B16 tumors.

For (L)–(N), at least six tumors were used in each group. Each experiment was repeated three times. Values are shown as mean ± SEM. *$p < 0.05$. NS, non-significant. See also Figures S3 and S4.

differences in experimental settings and make an accurate comparison between all mice groups, we performed an experiment combining all mice genotypes. We evaluated B16 tumor growth kinetics (Figure S6A) and B16 metastatic formation (Figure S6B), as well as D122 tumor growth kinetics (Figure S6C) and metastatic formation (Figure S6D) and observed that in all cases Ncr1 did not affect primary tumor growth. In contrast, metastases formation was Ncr1 dependent as in its absence increased metastases were detected, while upon its overexpression metastases formation decreased (Figures S6B and S6D).

NK cells and T cells are the main source of IFN-γ (Desbois et al., 2012; Fauriat et al., 2010; Garber, 2016; Morvan and Lanier, 2016). To demonstrate that NK cell-derived IFN-γ is responsible for the observed effects, we inoculated a control group (a group including *Ncr1*$^{+/gfp}$ and the non-transgenic littermates of Ncr1^{cre} Ncr1^{OE} mice), *Ncr1*$^{gfp/gfp}$, *Ifng*$^{-/-}$, and Ncr1^{cre} Ncr1^{OE} mice with B16 tumors. A day prior to tumor inoculation and every third day after until the time of RCM, the control mice were injected with either an anti-NK1.1-depleting antibody (to deplete NK cells) (Figure S6E) or an anti-CD3-depleting antibody (to deplete T cells) (Figure S6F).

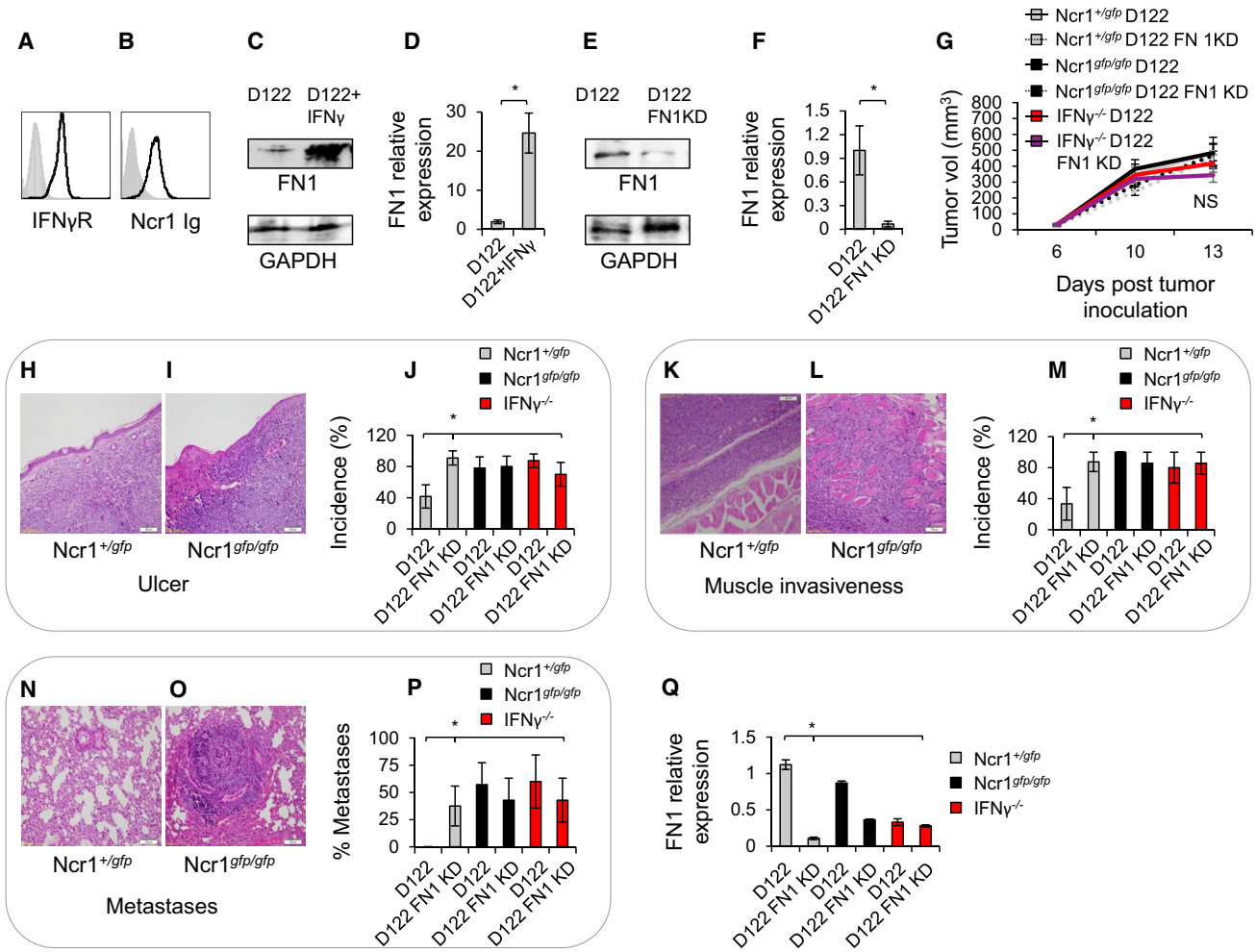

Figure 4. Ncr1 Edits D122 Structure via IFN-γ and FN1

(A and B) FACS staining of D122 cells. Black indicates specific staining; gray indicates background control. Each FACS plot is representative of three independent experiments.

(C and E) WB figures are representative of three experiments. To facilitate visualization, contrast was adjusted.

(D and F) qRT-PCR assays were performed on triplicates, normalized to GAPDH and ACTB. Each experiment was repeated three times. Values are shown as mean ± SEM.

(G) Tumor volume following s.c. inoculation of 1×10^6 D122 cells.

(H–P) Hematoxylin and eosin (H&E) staining of paraffin-embedded slides (H, I, K, L, N, O), quantified in (J), (M), and (P).

For (G)–(P), ten mice were used in each group. Values are shown as mean ± SEM.

(Q) qRT-PCR performed on triplicates, normalized to GAPDH and ACTB. Six tumors were used in each group. Values are shown as mean ± SEM. *$p < 0.05$. NS, non-significant.

See also Figure S5.

Depletion was verified by flow cytometry at different time points along the experiment. Additionally, a control group was administered an anti-IFN-γ blocking antibody. Mice were also treated with recombinant IFN-γ or left untreated (Figure 6). Tumors in all mice groups developed at a comparable rate and reached a similar final volume (Figure 6A). Increased metastases were observed in NK1.1- but not in CD3-depleted mice (Figure 6B). Moreover, increased metastases formation was observed also when blocking IFN-γ antibodies were used or in *Ifng*$^{-/-}$ mice.

Recombinant IFN-γ administration reduced metastases in all groups (Figure 6B). Likewise, in Ncr1^{cre} Ncr1^{OE} mice, metastases were significantly reduced (Figure 6B).

We next performed RCM evaluation (Figures 6C–6F). Worse RCM scores were recorded in the absence of Ncr1 (*Ncr1*$^{gfp/gfp}$), in the absence of NK cells (anti-NK1.1), or in the absence of IFN-γ (*Ifng*$^{-/-}$, anti-IFN-γ). The RCM scores were improved upon recombinant IFN-γ administration or in Ncr1 overexpression (Ncr1^{cre} Ncr1^{OE}) (Figures 6C–6F). These results indicate NK cells as the main source of IFN-γ in the tumors and NK cell-derived IFN-γ as the main player in modulating tumor structure and preventing metastasis, further corroborating the critical role of an Ncr1-IFN-γ-FN1 axis in metastases prevention.

FN1 is an important tumor marker and its upregulation in tumors is associated with an epithelial to mesenchymal transition

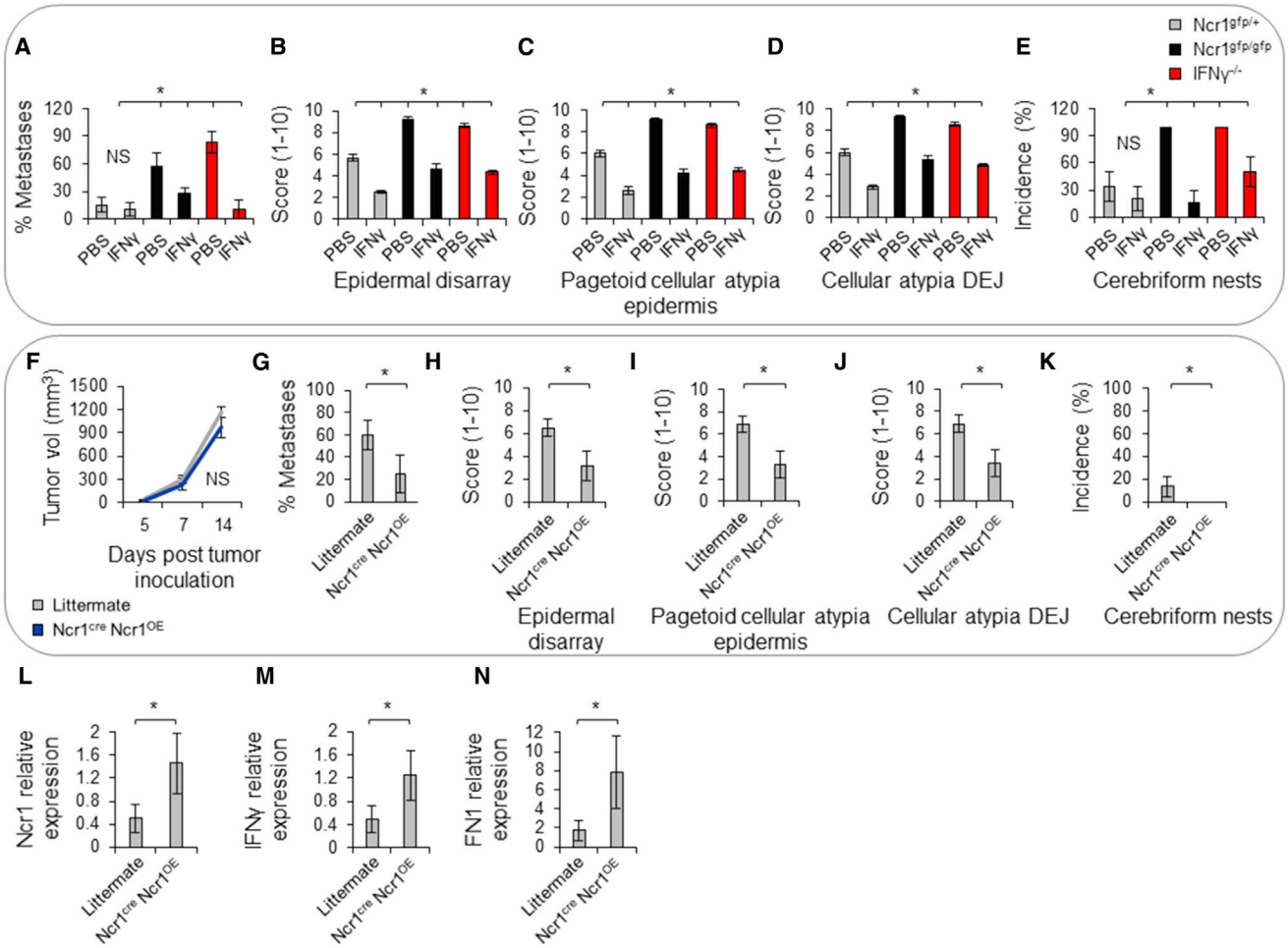

Figure 5. IFN-γ Administration and Ncr1 Overexpression Improves Mice Survival

(A) Mice were inoculated with B16 tumors, untreated (PBS) or treated with IFN-γ every third day from inoculation. Metastases were assessed, in animals bearing tumors of the same volume, at RCM.

(B–E) RCM features as indicated.

(F) Tumor volume following s.c. inoculation of 2×10^6 B16 cells in littermate controls and $Ncr1^{cre}$ $Ncr1^{OE}$ mice.

(G) Spontaneous metastasis in the animals presented in (F).

(H–K) RCM features as indicated.

For (A)–(K), at least eight animals were used in each group. Values are shown as mean ± SEM. *$p < 0.05$. NS, non-significant.

(L–N) qRT-PCR performed on B16 tumors. Four controls and five $Ncr1^{cre}$ $Ncr1^{OE}$ tumors were assessed. Values are shown as mean ± SEM.

See also Figure S6.

(EMT) profile and to the expression of various EMT-associated transcription factors (TFs). To investigate how FN1 contributes to the prevention of metastases, we inoculated $Ncr1^{+/gfp}$ and $Ncr1^{gfp/gfp}$ mice with B16 and D122 tumors and assessed the level of various EMT associated TFs at different time points following tumor inoculation. Figure S7 represents data obtained from tumors harvested at day 7 (day of RCM) after tumor inoculation. We found increased expression of Keratin (Figure S7A), N-Cadherin (N-CAD) (Figure S7B), SNAIL (Figure S7C), TWIST (Figure S7D), and Vimentin (Figure S7E) in the tumors of $Ncr1^{gfp/gfp}$ compared to $Ncr1^{+/gfp}$ mice. Similar results were observed for D122 tumors (Figures S7F–S7J). We thus concluded that an association to a reduced EMT profile may provide a partial mechanistic explanation as to the effect by which Ncr1-mediated IFN-γ secretion and FN1 induction in tumors prevents metastases in our model.

To extend our findings to humans, we initially stained various primary melanoma lines obtained from patients for the expression of IFN-γR (Figure 7A) and the unknown human NKp46 tumor ligand (Figure 7B) and observed expression of both in all tested tumors (Figures 7A and 7B).

We next analyzed datasets from patients of various cancers, including melanoma and carcinoma. Our analysis demonstrated that high expression of each of the tested genes alone: Ncr1 (Figure 7C), IFN-γ (Figure 7D), IFN-γR (Figure 7E), and FN1 (Figure 7F) was associated with statistically insignificant (Ncr1, IFN-γ IFN-γR, Figures 7C–7E) or statistically significant but small (FN1, Figure 7F) increase in survival rates. However, the combined

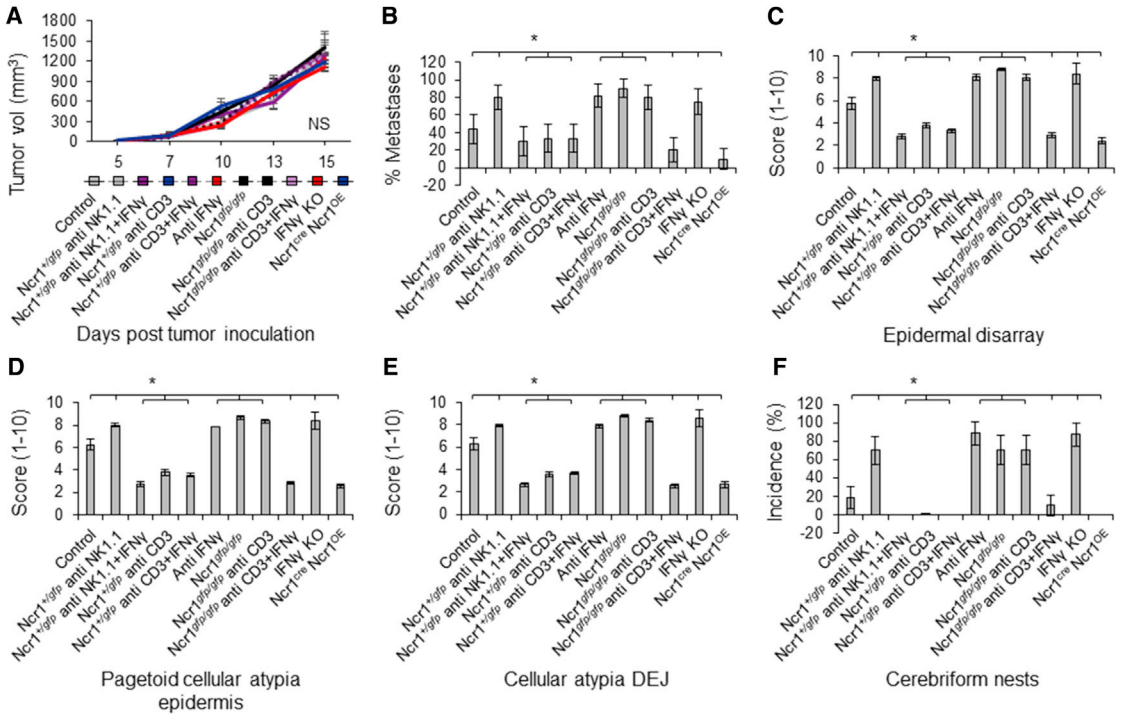

Figure 6. Tumor Development, Metastases, and RCM in the Absence of NK Cells, T Cells, or IFN-γ

(A) Tumor volume following s.c. inoculation of 1 × 10^6 B16 cells.

(B) Spontaneous metastasis in the same animals presented in (A).

(C–F) Quantification of the RCM features (described in STAR Methods) assessed on the tumors presented in (A). Scores: 1 = least aggressive to 10 = most aggressive. Ten mice were used in each group.

Values are shown as mean ± SEM. *p < 0.05. See also Figures S6 and S7.

expression of all genes in primary tumors correlated with significantly improved recurrence-free survival (Figures 7G and 7H).

DISCUSSION

We (Elboim et al., 2010; Glasner et al., 2012a; Halfteck et al., 2009) and others (Lakshmikanth et al., 2009) have demonstrated that NK cells, through the killer receptor NKp46, eliminate various tumor metastases. However, the mechanisms by which NKp46 and Ncr1, in mice, influence metastasis *in vivo* remain unknown. Here, we demonstrated that Ncr1 edits the structure of developing tumors at the level of tissue organization and that this effect is mediated by the IFN-γ-FN1 pathway. We further demonstrated that after this structural editing, metastases formation is restricted. We have previously demonstrated that Ncr1 control of various mouse tumors is mediated by direct killing rather than cytokine secretion (Glasner et al., 2012a). However, cytokine measurement in the previous study was performed after 48 and 76 hr of incubation with the targets (in contrast to 12 hr here), which may have been inappropriate, as IFN-γ and TNFα, the main NK cell cytokines, are secreted very rapidly and have a very short half-life (Fauriat et al., 2010).

By using RCM *in vivo*, which as opposed to conventional histological examination, enables *in situ* visualization of tumor architecture, we were able to determine that the killer receptor NKp46/Ncr1 affects melanoma tumors by modifying the tumors' structural properties. This effect was achieved through the secretion of IFN-γ and modulating tumor organization by upregulating the extracellular matrix protein FN1.

Pellacani et al. (2007) used RCM in humans and defined the aggressiveness of the tumors and their probability to metastasize. We observed that the B16 melanoma model is very similar to human melanoma, sharing similar RCM structural properties. In our RCM evaluation, we found the features of epidermal disarray, epidermal cellular atypia, dermal-epidermal junction cellular atypia, and dermal epidermal junction cerebriform like cell-clusters (nests) to be much more pronounced in primary tumors developed in the *Ncr1*$^{gfp/gfp}$ mice than in those developed in the *Ncr1*$^{+/gfp}$ mice. These criteria are particularly important as they are associated with melanomas thicker than 1 mm in depth (melanoma thickness is positively correlated to metastatic activity) (Wisco and Sober, 2012). This means that in the absence of Ncr1, tumors of the same developmental stage and volume feature more aggressive properties. Indeed, we observed significantly higher spontaneous metastasis in the absence of Ncr1.

To demonstrate that Ncr1-mediated induction of IFN-γ is the main element playing a role in these effects, we employed several different methods throughout our study. First, we used B16 tumors expressing very low levels of IFN-γR or an IFN-γ blocking antibody and observed significant worse metastasis and structural properties. Next, when depleting NK cells, but not T cells, we also observed worse metastases formation and worse structures in the developing tumors. Finally, administration of recombinant IFN-γ reversed these effects.

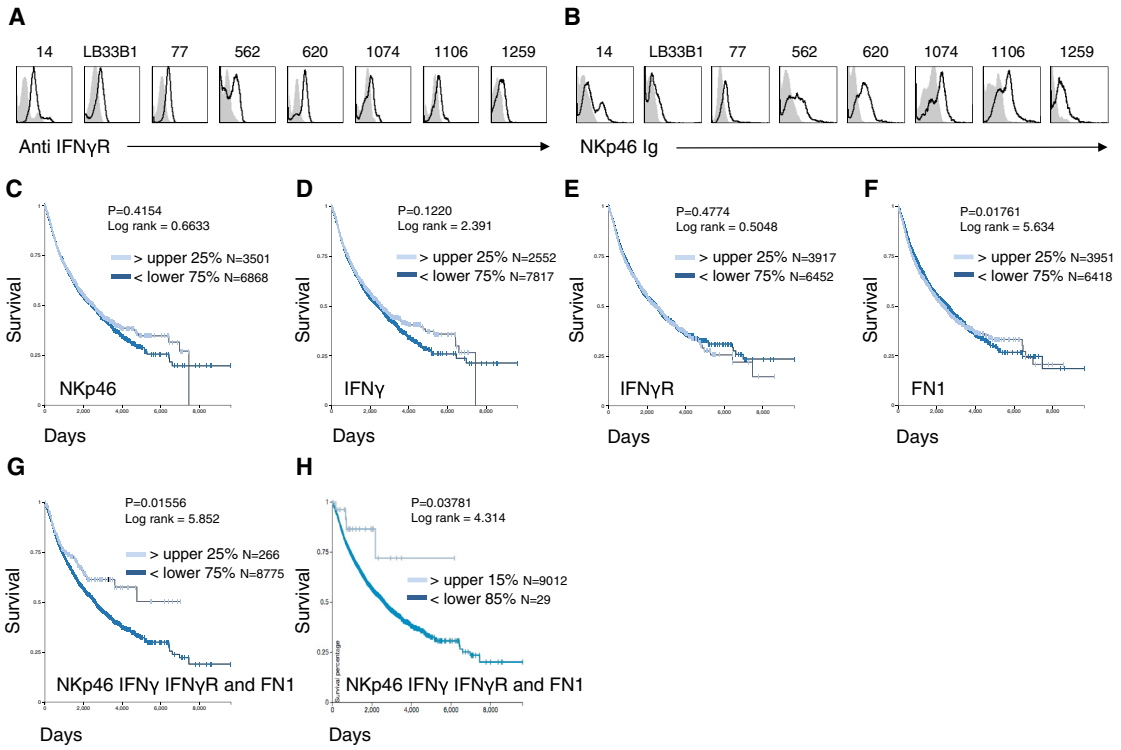

Figure 7. NKp46, IFN-γ, IFN-γR1, and FN1 Combined Expression in Human Tumors Is Prognostic of Better Survival

(A and B) FACS staining of primary human melanoma lines. Black indicates specific staining and gray indicates background control. The figure represents two independent stainings.

(C–H) Kaplan Meier analysis of survival in patients. Data were taken from the NIH TCGA PANCAN database. Analysis was performed using Xena UCSC. The figure compares high to low expression of NKp46 (C), IFN-γ (D), IFN-γR (E), and FN1 (F) alone or their combined high expression (G, H). Statistics is indicated within each plot.

The results presented here, demonstrating that Ncr1 inhibits the aggressiveness of the developing tumors via IFN-γ, are particularly important as triggering of Ncr1 may provide the only source of IFN-γ. $CD8^+$ T cells are often inhibited at the sites of tumors, due to MHC class I downregulation. For example, in about 67% of human melanomas, MHC class I expression is downregulated via various mechanisms (Degenhardt et al., 2010) and thus the secretion of IFN-γ from CTLs is prevented. Furthermore, many human melanomas do not express NKG2D ligands (Fuertes et al., 2008) and therefore NKG2D, one of the other major NK cell receptors involved in IFN-γ secretion, cannot be activated. Ncr1 is also expressed by ILCs, although its function on these cells was shown to be redundant (Rankin et al., 2016; Satoh-Takayama et al., 2009).

We demonstrated that editing of tumor architecture by Ncr1 is not restricted to a particular cell line or tumor type, as we showed that Ncr1 affects the structural properties and metastasis of D122 in an IFN-γ- and FN1-dependent manner. Furthermore, we were able to generalize our findings to a wide range of human tumors, by analyzing human patients' data files using the NIH TCGA database. Importantly, *post hoc* analysis of TCGA data has many caveats and these data should be considered as hypothesis generating.

Most of the above-mentioned activities of Ncr1 were demonstrated via the *Ncr1*$^{gfp/gfp}$ mice (Gazit et al., 2006). To determine the therapeutic potential of our findings, we used a transgenic mouse in which Ncr1 is overexpressed in NK cells ($Ncr1^{cre}$ $Ncr1^{OE}$) (Glasner et al., 2017). In these transgenic mice, tumor architecture assessed by RCM imaging was found to be better than in the non-transgenic littermates and led to fewer metastases formation via the same IFN-γ-FN1 pathway. These observations suggest that overexpression of NKp46 in NK cells may provide an important perspective for NK cell immunotherapy.

We demonstrated here that Ncr1 impedes metastases via editing of primary tumors in an IFN-γ-FN1-dependent manner. However, FN1 involvement in tumor development is complex. FN1 is upregulated in various cancers, including mouse and human metastatic melanomas (Clark et al., 2000; Kudo-Saito et al., 2009; Sengupta et al., 2010). FN1 is also an important mesenchymal gene associated with a reduction in E-cadherin levels and increase in N-CAD, Vimentin, and other TFs associated with EMT and metastasis (Lamouille et al., 2014). On the other hand, FN1 was found to inhibit tumor growth and metastasis (Liu et al., 2008; Yi and Ruoslahti, 2001). Failure to deposit stromal FN1 by the tumors was correlated to higher migration, invasion, and metastatic activity (Liu et al., 2008). Reduced FN1 levels were reported at the peripheral margins of invading tumors and FN1 silencing in some tumors enhanced tumor growth as well as promoted lung metastases (Liu et al., 2008). Correspondingly, FN1 expression was higher in poorly metastatic lines

isolated from patients, compared to the higher metastatic ones, in an immunodeficient mouse xenotransplant metastasis model (Xu et al., 2008). Clearly, FN1 is a prominent tumor marker important for many tumor processes. However, FN1 presence in the tumors is dynamic, and its expression at certain loci or time points in tumor development may direct metastatic activity. Possibly, the association of FN1 expression in tumors with an increased EMT profile documents the result of a complex interaction between the immune system and the tumor.

In summary, our observations indicate that even in the early pre-metastatic stage, the tumor ''prepares'' itself to disseminate and that even at this stage NK cells, via Ncr1-mediated secretion of IFN-γ, attempt to counter these morphological changes. The finding that Ncr1, through IFN-γ and FN1, is involved in modifying tumor organization and consequently restricting metastasis represents a potential avenue for treatment. This paradigm may pave the way to anti-cancer treatment options and to the development of drugs specifically aimed at targeting tumor architecture.

STAR★METHODS

Detailed methods are provided in the online version of this paper and include the following:

- KEY RESOURCES TABLE
- CONTACT FOR REAGENT AND RESOURCE SHARING
- EXPERIMENTAL MODEL AND SUBJECT DETAILS
  - Mice, tumor development and metastasis
  - Cells
- METHOD DETAILS
  - Fusion proteins, antibodies, and flow cytometry
  - CD107a degranulation and cytokine secretion assays
  - Evaluation by RCM
  - RCM examination of human melanomas
  - Quantitative PCR (qRT-PCR) and Western Blotting (WB)
  - RNA isolation and library construction for transcriptome analysis
  - Processing and Analysis of RNA-Seq Data
  - Preparation of cryosections and immunofluorescence staining
- QUANTIFICATION AND STATISTICAL ANALYSIS
- DATA AND SOFTWARE AVAILABILITY
- ADDITIONAL RESOURCES

SUPPLEMENTAL INFORMATION

Supplemental Information includes seven figures and can be found with this article online at https://doi.org/10.1016/j.immuni.2017.12.007.

ACKNOWLEDGMENTS

This work was supported by the European Research Council under the European Union's Seventh Framework Programme (FP/2007-2013)/ERC Grant Agreement number 320473-BacNK. Further support came from the Israel Science Foundation, the GIF foundation (to O.M. and B.S.), the ICRF professorship grant, the Helmhultz foundation, and the Rosetrees Trust (all to O.M.). O.M. is a Crown Professor of Molecular Immunology. A.G. and A.L. were supported by a grant from the joint research fund of the Hebrew University and Hadassah Medical Center. J.H.H. is a New York Stem Cell Foundation (NYSCF)-Robertson Investigator. V.S. is supported by SFB-61. L.Z. is supported by PLBIO INCA 2016. B.S. is supported by the GRK1591 grant and the Cancer Aid grants #31113557 and #34102500.

AUTHOR CONTRIBUTIONS

A.G. designed and performed the experiments, analyzed the data, and wrote the manuscript. A.L. performed RCM evaluation and analysis. J.E. and B.I. assisted with performing the experiments. S.O., A.S., T.N., and C.D.E. assisted with analysis of the data. S.V., J.H.H., and V.S. contributed to generating the transgenic mice. S.J. contributed reagents. B.S. and L.Z. contributed essential ideas and discussion. O.M. supervised the work and wrote the manuscript.

DECLARATION OF INTEREST STATEMENT

The authors declare no competing interests.

Received: April 11, 2017
Revised: August 15, 2017
Accepted: December 5, 2017
Published: January 9, 2018; corrected online: January 17, 2018

REFERENCES

Arnold, M., Holterhues, C., Hollestein, L.M., Coebergh, J.W., Nijsten, T., Pukkala, E., Holleczek, B., Tryggvadóttir, L., Comber, H., Bento, M.J., et al. (2014). Trends in incidence and predictions of cutaneous melanoma across Europe up to 2015. J. Eur. Acad. Dermatol. Venereol. *28*, 1170–1178.

Bar-On, Y., Glasner, A., Meningher, T., Achdout, H., Gur, C., Lankry, D., Vitenshtein, A., Meyers, A.F.A., Mandelboim, M., and Mandelboim, O. (2013). Neuraminidase-mediated, NKp46-dependent immune-evasion mechanism of influenza viruses. Cell Rep. *3*, 1044–1050.

Bar-On, Y., Seidel, E., Tsukerman, P., Mandelboim, M., and Mandelboim, O. (2014). Influenza virus uses its neuraminidase protein to evade the recognition of two activating NK cell receptors. J. Infect. Dis. *210*, 410–418.

Breunis, W.B., Tarazona-Santos, E., Chen, R., Kiley, M., Rosenberg, S.A., and Chanock, S.J. (2008). Influence of cytotoxic T lymphocyte-associated antigen 4 (CTLA4) common polymorphisms on outcome in treatment of melanoma patients with CTLA-4 blockade. J. Immunother. *31*, 586–590.

Chaushu, S., Wilensky, A., Gur, C., Shapira, L., Elboim, M., Halftek, G., Polak, D., Achdout, H., Bachrach, G., and Mandelboim, O. (2012). Direct recognition of Fusobacterium nucleatum by the NK cell natural cytotoxicity receptor NKp46 aggravates periodontal disease. PLoS Pathog. *8*, e1002601.

Chernyavskiy, O., Vannucci, L., Bianchini, P., Difato, F., Saieh, M., and Kubínová, L. (2009). Imaging of mouse experimental melanoma in vivo and ex vivo by combination of confocal and nonlinear microscopy. Microsc. Res. Tech. *72*, 411–423.

Clark, E.A., Golub, T.R., Lander, E.S., and Hynes, R.O. (2000). Genomic analysis of metastasis reveals an essential role for RhoC. Nature *406*, 532–535.

Degenhardt, Y., Huang, J., Greshock, J., Horiates, G., Nathanson, K., Yang, X., Herlyn, M., and Weber, B. (2010). Distinct MHC gene expression patterns during progression of melanoma. Genes Chromosomes Cancer *49*, 144–154.

Delahaye, N.F., Rusakiewicz, S., Martins, I., Ménard, C., Roux, S., Lyonnet, L., Paul, P., Sarabi, M., Chaput, N., Semeraro, M., et al. (2011). Alternatively spliced NKp30 isoforms affect the prognosis of gastrointestinal stromal tumors. Nat. Med. *17*, 700–707.

Desbois, M., Rusakiewicz, S., Locher, C., Zitvogel, L., and Chaput, N. (2012). Natural killer cells in non-hematopoietic malignancies. Front. Immunol. *3*, 395.

Diab, M., Vitenshtein, A., Drori, Y., Yamin, R., Danziger, O., Zamostiano, R., Mandelboim, M., Bacharach, E., and Mandelboim, O. (2016). Suppression of human metapneumovirus (HMPV) infection by the innate sensing gene CEACAM1. Oncotarget *7*, 66468–66479.

Diab, M., Glasner, A., Isaacson, B., Bar-On, Y., Drori, Y., Yamin, R., Duev-Cohen, A., Danziger, O., Zamostiano, R., Mandelboim, M., et al. (2017). NK-cell receptors NKp46 and NCR1 control human metapneumovirus infection. Eur. J. Immunol. *47*, 692–703.

Draghi, M., Pashine, A., Sanjanwala, B., Gendzekhadze, K., Cantoni, C., Cosman, D., Moretta, A., Valiante, N.M., and Parham, P. (2007). NKp46 and NKG2D recognition of infected dendritic cells is necessary for NK cell activation in the human response to influenza infection. J. Immunol. *178*, 2688–2698.

Eckelhart, E., Warsch, W., Zebedin, E., Simma, O., Stoiber, D., Kolbe, T., Rülicke, T., Mueller, M., Casanova, E., and Sexl, V. (2011). A novel Ncr1-Cre mouse reveals the essential role of STAT5 for NK-cell survival and development. Blood *117*, 1565–1573.

Eisenbach, L., Ramanathan, R., and Nelson, D.L. (1983a). Biochemical studies of the excitable membrane of paramecium tetraurelia. IX. Antibodies against ciliary membrane proteins. J. Cell Biol. *97*, 1412–1420.

Eisenbach, L., Segal, S., and Feldman, M. (1983b). MHC imbalance and metastatic spread in Lewis lung carcinoma clones. Int. J. Cancer *32*, 113–120.

Elboim, M., Gazit, R., Gur, C., Ghadially, H., Betser-Cohen, G., and Mandelboim, O. (2010). Tumor immunoediting by NKp46. J. Immunol. *184*, 5637–5644.

Fauriat, C., Long, E.O., Ljunggren, H.G., and Bryceson, Y.T. (2010). Regulation of human NK-cell cytokine and chemokine production by target cell recognition. Blood *115*, 2167–2176.

Flaherty, K.T., Puzanov, I., Kim, K.B., Ribas, A., McArthur, G.A., Sosman, J.A., O'Dwyer, P.J., Lee, R.J., Grippo, J.F., Nolop, K., and Chapman, P.B. (2010). Inhibition of mutated, activated BRAF in metastatic melanoma. N. Engl. J. Med. *363*, 809–819.

Fuertes, M.B., Girart, M.V., Molinero, L.L., Domaica, C.I., Rossi, L.E., Barrio, M.M., Mordoh, J., Rabinovich, G.A., and Zwirner, N.W. (2008). Intracellular retention of the NKG2D ligand MHC class I chain-related gene A in human melanomas confers immune privilege and prevents NK cell-mediated cytotoxicity. J. Immunol. *180*, 4606–4614.

Garber, K. (2016). Natural killer cells blaze into immuno-oncology. Nat. Biotechnol. *34*, 219–220.

Gazit, R., Gruda, R., Elboim, M., Arnon, T.I., Katz, G., Achdout, H., Hanna, J., Qimron, U., Landau, G., Greenbaum, E., et al. (2006). Lethal influenza infection in the absence of the natural killer cell receptor gene Ncr1. Nat. Immunol. *7*, 517–523.

Ghadially, H., Horani, A., Glasner, A., Elboim, M., Gazit, R., Shoseyov, D., and Mandelboim, O. (2013). NKp46 regulates allergic responses. Eur. J. Immunol. *43*, 3006–3016.

Ghadially, H., Ohana, M., Elboim, M., Gazit, R., Gur, C., Nagler, A., and Mandelboim, O. (2014). NK cell receptor NKp46 regulates graft-versus-host disease. Cell Rep. *7*, 1809–1814.

Glasner, A., Ghadially, H., Gur, C., Stanietsky, N., Tsukerman, P., Enk, J., and Mandelboim, O. (2012a). Recognition and prevention of tumor metastasis by the NK receptor NKp46/NCR1. J. Immunol. *188*, 2509–2515.

Glasner, A., Zurunic, A., Meningher, T., Lenac Rovis, T., Tsukerman, P., Bar-On, Y., Yamin, R., Meyers, A.F., Mandeboim, M., Jonjic, S., and Mandelboim, O. (2012b). Elucidating the mechanisms of influenza virus recognition by Ncr1. PLoS ONE *7*, e36837.

Glasner, A., Roth, Z., Varvak, A., Miletic, A., Isaacson, B., Bar-On, Y., Jonjic, S., Khalaila, I., and Mandelboim, O. (2015a). Identification of putative novel O-glycosylations in the NK killer receptor Ncr1 essential for its activity. Cell Discov. *1*, 15036.

Glasner, A., Simic, H., Miklić, K., Roth, Z., Berhani, O., Khalaila, I., Jonjic, S., and Mandelboim, O. (2015b). Expression, function, and molecular properties of the killer receptor Ncr1-Noé. J. Immunol. *195*, 3959–3969.

Glasner, A., Isaacson, B., Viukov, S., Neuman, T., Friedman, N., Mandelboim, M., Sexl, V., Hanna, J.H., and Mandelboim, O. (2017). Increased NK cell immunity in a transgenic mouse model of NKp46 overexpression. Sci. Rep. *7*, 13090.

Gur, C., Porgador, A., Elboim, M., Gazit, R., Mizrahi, S., Stern-Ginossar, N., Achdout, H., Ghadially, H., Dor, Y., Nir, T., et al. (2010). The activating receptor NKp46 is essential for the development of type 1 diabetes. Nat. Immunol. *11*, 121–128.

Gur, C., Enk, J., Kassem, S.A., Suissa, Y., Magenheim, J., Stolovich-Rain, M., Nir, T., Achdout, H., Glaser, B., Shapiro, J., et al. (2011). Recognition and killing of human and murine pancreatic beta cells by the NK receptor NKp46. J. Immunol. *187*, 3096–3103.

Gur, C., Doron, S., Kfir-Erenfeld, S., Horwitz, E., Abu-Tair, L., Safadi, R., and Mandelboim, O. (2012). NKp46-mediated killing of human and mouse hepatic stellate cells attenuates liver fibrosis. Gut *61*, 885–893.

Gur, C., Coppenhagen-Glazer, S., Rosenberg, S., Yamin, R., Enk, J., Glasner, A., Bar-On, Y., Fleissig, O., Naor, R., Abed, J., et al. (2013a). Natural killer cell-mediated host defense against uropathogenic E. coli is counteracted by bacterial hemolysinA-dependent killing of NK cells. Cell Host Microbe *14*, 664–674.

Gur, C., Enk, J., Weitman, E., Bachar, E., Suissa, Y., Cohen, G., Schyr, R.B., Sabanay, H., Horwitz, E., Glaser, B., et al. (2013b). The expression of the beta cell-derived autoimmune ligand for the killer receptor nkp46 is attenuated in type 2 diabetes. PLoS ONE *8*, e74033.

Gur, C., Ibrahim, Y., Isaacson, B., Yamin, R., Abed, J., Gamliel, M., Enk, J., Bar-On, Y., Stanietsky-Kaynan, N., Coppenhagen-Glazer, S., et al. (2015). Binding of the Fap2 protein of Fusobacterium nucleatum to human inhibitory receptor TIGIT protects tumors from immune cell attack. Immunity *42*, 344–355.

Guy, G.P., and Ekwueme, D.U. (2011). Years of potential life lost and indirect costs of melanoma and non-melanoma skin cancer: a systematic review of the literature. Pharmacoeconomics *29*, 863–874.

Halfteck, G.G., Elboim, M., Gur, C., Achdout, H., Ghadially, H., and Mandelboim, O. (2009). Enhanced in vivo growth of lymphoma tumors in the absence of the NK-activating receptor NKp46/NCR1. J. Immunol. *182*, 2221–2230.

Jarahian, M., Watzl, C., Fournier, P., Arnold, A., Djandji, D., Zahedi, S., Cerwenka, A., Paschen, A., Schirrmacher, V., and Momburg, F. (2009). Activation of natural killer cells by newcastle disease virus hemagglutinin-neuraminidase. J. Virol. *83*, 8108–8121.

Jarahian, M., Fiedler, M., Cohnen, A., Djandji, D., Hämmerling, G.J., Gati, C., Cerwenka, A., Turner, P.C., Moyer, R.W., Watzl, C., et al. (2011). Modulation of NKp30- and NKp46-mediated natural killer cell responses by poxviral hemagglutinin. PLoS Pathog. *7*, e1002195.

Koch, J., Steinle, A., Watzl, C., and Mandelboim, O. (2013). Activating natural cytotoxicity receptors of natural killer cells in cancer and infection. Trends Immunol. *34*, 182–191.

Kudo-Saito, C., Shirako, H., Takeuchi, T., and Kawakami, Y. (2009). Cancer metastasis is accelerated through immunosuppression during Snail-induced EMT of cancer cells. Cancer Cell *15*, 195–206.

Lakshmikanth, T., Burke, S., Ali, T.H., Kimpfler, S., Ursini, F., Ruggeri, L., Capanni, M., Umansky, V., Paschen, A., Sucker, A., et al. (2009). NCRs and DNAM-1 mediate NK cell recognition and lysis of human and mouse melanoma cell lines in vitro and in vivo. J. Clin. Invest. *119*, 1251–1263.

Lamouille, S., Xu, J., and Derynck, R. (2014). Molecular mechanisms of epithelial-mesenchymal transition. Nat. Rev. Mol. Cell Biol. *15*, 178–196.

Li, Y., Gonzalez, S., Terwey, T.H., Wolchok, J., Li, Y., Aranda, I., Toledo-Crow, R., and Halpern, A.C. (2005). Dual mode reflectance and fluorescence confocal laser scanning microscopy for in vivo imaging melanoma progression in murine skin. J. Invest. Dermatol. *125*, 798–804.

Liu, W., Cheng, S., Asa, S.L., and Ezzat, S. (2008). The melanoma-associated antigen A3 mediates fibronectin-controlled cancer progression and metastasis. Cancer Res. *68*, 8104–8112.

Mandelboim, O., Lieberman, N., Lev, M., Paul, L., Arnon, T.I., Bushkin, Y., Davis, D.M., Strominger, J.L., Yewdell, J.W., and Porgador, A. (2001). Recognition of haemagglutinins on virus-infected cells by NKp46 activates lysis by human NK cells. Nature *409*, 1055–1060.

Morvan, M.G., and Lanier, L.L. (2016). NK cells and cancer: you can teach innate cells new tricks. Nat. Rev. Cancer *16*, 7–19.

Parakh, S., Park, J.J., Mendis, S., Rai, R., Xu, W., Lo, S., Drummond, M., Rowe, C., Wong, A., McArthur, G., et al. (2017). Efficacy of anti-PD-1 therapy in patients with melanoma brain metastases. Br. J. Cancer *116*, 1558–1563.

Park, J., Mroz, P., Hamblin, M.R., and Yaroslavsky, A.N. (2010). Dye-enhanced multimodal confocal microscopy for noninvasive detection of skin cancers in mouse models. J. Biomed. Opt. *15*, 026023.

Pellacani, G., Guitera, P., Longo, C., Avramidis, M., Seidenari, S., and Menzies, S. (2007). The impact of in vivo reflectance confocal microscopy for the diagnostic accuracy of melanoma and equivocal melanocytic lesions. J. Invest. Dermatol. *127*, 2759–2765.

Porgador, A., Feldman, M., and Eisenbach, L. (1989). H-2Kb transfection of B16 melanoma cells results in reduced tumourigenicity and metastatic competence. J. Immunogenet. *16*, 291–303.

Rankin, L.C., Girard-Madoux, M.J., Seillet, C., Mielke, L.A., Kerdiles, Y., Fenis, A., Wieduwild, E., Putoczki, T., Mondot, S., Lantz, O., et al. (2016). Complementarity and redundancy of IL-22-producing innate lymphoid cells. Nat. Immunol. *17*, 179–186.

Satoh-Takayama, N., Dumoutier, L., Lesjean-Pottier, S., Ribeiro, V.S., Mandelboim, O., Renauld, J.C., Vosshenrich, C.A., and Di Santo, J.P. (2009). The natural cytotoxicity receptor NKp46 is dispensable for IL-22-mediated innate intestinal immune defense against *Citrobacter rodentium*. J. Immunol. *183*, 6579–6587.

Seidel, E., Glasner, A., and Mandelboim, O. (2012). Virus-mediated inhibition of natural cytotoxicity receptor recognition. Cell. Mol. Life Sci. *69*, 3911–3920.

Sengupta, S., Nandi, S., Hindi, E.S., Wainwright, D.A., Han, Y., and Lesniak, M.S. (2010). Short hairpin RNA-mediated fibronectin knockdown delays tumor growth in a mouse glioma model. Neoplasia *12*, 837–847.

Sheppard, S., Triulzi, C., Ardolino, M., Serna, D., Zhang, L., Raulet, D.H., and Guerra, N. (2013). Characterization of a novel NKG2D and NKp46 double-mutant mouse reveals subtle variations in the NK cell repertoire. Blood *121*, 5025–5033.

Vitenshtein, A., Charpak-Amikam, Y., Yamin, R., Bauman, Y., Isaacson, B., Stein, N., Berhani, O., Dassa, L., Gamliel, M., Gur, C., et al. (2016). NK cell recognition of *Candida glabrata* through binding of NKp46 and NCR1 to fungal ligands Epa1, Epa6, and Epa7. Cell Host Microbe *20*, 527–534.

Wensveen, F.M., Jelenčić, V., Valentić, S., Šestan, M., Wensveen, T.T., Theurich, S., Glasner, A., Mendrila, D., Štimac, D., Wunderlich, F.T., et al. (2015). NK cells link obesity-induced adipose stress to inflammation and insulin resistance. Nat. Immunol. *16*, 376–385.

Wisco, O.J., and Sober, A.J. (2012). Prognostic factors for melanoma. Dermatol. Clin. *30*, 469–485.

Xu, L., Shen, S.S., Hoshida, Y., Subramanian, A., Ross, K., Brunet, J.P., Wagner, S.N., Ramaswamy, S., Mesirov, J.P., and Hynes, R.O. (2008). Gene expression changes in an animal melanoma model correlate with aggressiveness of human melanoma metastases. Mol. Cancer Res. *6*, 760–769.

Yi, M., and Ruoslahti, E. (2001). A fibronectin fragment inhibits tumor growth, angiogenesis, and metastasis. Proc. Natl. Acad. Sci. USA *98*, 620–624.

STAR★METHODS

KEY RESOURCES TABLE

REAGENT or RESOURCE	SOURCE	IDENTIFIER
Antibodies		
Alexa Fluor 647 conjugated goat anti human IgG, F(ab')$_2$	JacksonImmunoResearch Laboratories, West Grove, PA	Cat#109-606-097
Alexa Fluor 647 streptavidin	JacksonImmunoResearch Laboratories, West Grove, PA	Cat#016-600-084
Alexa Fluor 647 conjugated goat anti mouse IgG (H+L)	JacksonImmunoResearch Laboratories, West Grove, PA	Cat#115-095-062
Biotin anti mouse CD119 (IFN-γR α chain),	Bioledgend (Enco Israel)	Cat#112803
Purified anti mouse TNFα	Bioledgend (Enco Israel)	Cat#506301
Polyclonal FN1	abcam (Zotal, Isreal)	Cat#ab2413
Anti mNcr1.15	Prof. Stipan Jonjic (University of Rijeka, B. Branchetta, Rijeka, Croatia)	Glasner et al. (2015a, 2015b)
InVivoMAb anti mouse NK1.1, clone PK136.	Bio X Cell	Cat#BE0036-5
InVivoMAb anti mouse CD3ε, clone 145-2C11	Bio X Cell	Cat#BE0001-1
InVivoMAb anti mouse IFN-γ, clone XMG1.2	Bio X Cell	Cat#BE0055-25
APC anti mouse CD107a (LAMP-1)	Biotest (Enco Israel)	Cat#121614
Chemicals, Peptides, and Recombinant Proteins		
Proteinase K	Sigma-Aldrich (Rehovot, Israel)	Cat#P2308
Neuraminidase	Mercury, Israel	Cat#MBS480716250MI
Recombinant IFN-γ (carrier free)	Bioledgend (Enco Israel)	Cat#575302
Critical Commercial Assays		
TrueSeq RNA V2 kit	Illumina	Cat#RS-122-2001 /2
EasySep mouse NKcell isolation kit	STEMCELL (Enco Israel)	Cat#19855
Deposited Data		
RNA seq of IFN-γ treated and untreated B16 cells	This paper	GEO: GSE106390
Experimental Models: Cell Lines		
B16F10.9	Prof. Eisenbach (The Weizmann Institute of Science, Rehovot, Israel)	Porgador et al. (1989)
D122	Prof. Eisenbach (The Weizmann Institute of Science, Rehovot, Israel)	Eisenbach et al. (1983b)
Experimental Models: Organisms/Strains		
IFN-γ−/− mice, B6.129S7-IFN-gtm1Ts/J	the Jackson Laboratory (Bar Harbor, ME)	Cat#002287
TNFα−/− mice, B6;129S-Tnftm1Gkl/J	the Jackson Laboratory (Bar Harbor, ME)	Cat#003008
Ncr1^{cre} Ncr1^{OE}	This paper	N/A
Ncr1$^{+/gfp}$, Ncr1$^{gfp/gfp}$	Gazit et al. (2006)	Cat#022739

CONTACT FOR REAGENT AND RESOURCE SHARING

Further information and requests for resources and reagents should be directed to and will be fulfilled by the Lead Contact, Ofer Mandelboim (oferm@ekmd.huji.ac.il).

EXPERIMENTAL MODEL AND SUBJECT DETAILS

Mice, tumor development and metastasis

All experiments were performed using 6–8 weeks old C57BL/6 male and female mice. The generation of the Ncr1$^{gfp/gfp}$ mouse was described previously (Gazit et al., 2006). Ncr1$^{+/gfp}$ and Ncr1$^{gfp/gfp}$ mice possess normal numbers of NK cells and their NK cell

education is normal (Gazit et al., 2006; Glasner et al., 2015b; Satoh-Takayama et al., 2009; Sheppard et al., 2013) IFN-$\gamma^{-/-}$ and TNF$\alpha^{-/-}$ mice were purchased from the Jackson Laboratory (Bar Harbor, ME). Ncr1^{cre} Ncr1^{OE} mice were generated by crossing Ncr1^{cre} (Eckelhart et al., 2011) and Ncr1 Rosa Stop mice (Glasner et al., 2017). All mice were housed under SPF conditions, normal light/dark cycles and 22$^{+/-}$2°C. All experiments were performed in a specific pathogen free unit of the Hebrew University Medical School (Ein-Kerem, Jerusalem) in accordance with the guidelines of the ethics committee. Mice of different genotypes (or littermates when relevant) were allocated randomly to the different experimental groups in each experiment. Peritoneal tumor growth was assessed by injecting 10-fold decreasing dose of B16 cells into the peritoneal cavity of Ncr1$^{+/gfp}$ and Ncr1$^{gfp/gfp}$ mice. The mice were monitored daily, and sacrificed at any indication of illness such as bristled fur, difficult breathing, tremor or any other sign of disease. The sacrificed mice chest and peritoneal cavities were explored post-mortem, and the presence of tumors was visually verified. Any surviving mice were sacrificed at day 120 post tumor inoculation, their chest cavities were explored and the absence of metastases was verified by visual inspection. For RCM evaluation, histopathological analysis and spontaneous metastases assessment, B16 or D122 cells were subcutaneously (s.c.) injected into the flank and tumors were monitored daily. RCM evaluation and histopathological analysis were always conducted in a blinded manner, where the evaluating physician inspected randomly-numbered coded image files or numbered H&E stained slides with no indication of the animal's genotype.

In all experiments, by the time tumors reached a maximal volume of 1000mm^3, all mice were sacrificed and the presence of metastases in the peritoneum and chest cavity was assessed visually. No differences were observed between the various mice groups in their general health at baseline.

Cells

Male B16F10.9 (B16) cells and D122 Lewis Lung Carcinoma (D122) were kindly provided by Prof. Eisenbach (The Weizmann Institute of Science, Rehovot, Israel). Cells were authenticated. Cells were grown in DMEM supplemented with 1% L-glutamine, 1% non-essential amino acids, 1% sodium pyruvate, 1% pen strep and 5% FCS. Cells were grown in 37°C, 5% CO2. To obtain cell lines from the B16 tumors of Ncr1$^{+/gfp}$ and Ncr1$^{gfp/gfp}$ mice, tissue samples were treated with trypsin, washed and placed in culture. Two days later, tissues were removed and cells were grown in supplemented DMEM. All cells were stained for the expression of Ncr1 ligand within one week in culture at most. PK treatment included 20 min incubation of the cells with 10ml PK (20 mg/ml); Sigma-Aldrich, Rehovot, Israel) in 37°C, 5% CO2.

METHOD DETAILS

Fusion proteins, antibodies, and flow cytometry

The Ncr1 Ig and NKp46 Ig fusion proteins were generated by PCR amplification of mouse and human cDNA, and cloned in frame with human IgG. The resulting constructs were transduced into HEK293T cells. Treatment of fusion proteins with NA included incubation with 10ug NA (Mercury, Israel) for 2 hours at 37°C. The integrity of the treated fusion proteins was assessed by sodium dodecyl sulfate–polyacrylamide gel electrophoresis (SDS-PAGE) gel analysis. The staining of all cell lines by fusion proteins was visualized using an Alexa Fluor® 647 conjugated Goat Anti-Human IgG, F(ab')$_2$ (JacksonImmunoResearch Laboratories, West Grove, PA). To assess IFN-γR, biotin anti-mouse CD119 (IFN-γR α chain), (BioLegend) was used. To asses TNFαR, purified anti-mouse TNFα Antibody (BioLegend) was used. IFN-γR and TNFαR staining was visualized using Alexa Fluor® 647 Streptavidin, or Alexa Fluor® 647 conjugated Goat Anti-Mouse IgG (H+L) secondary antibodies (JacksonImmunoResearch Laboratories, West Grove, PA), respectively. mNcr1.15was used as a blocking anti-Ncr1 antibody. Polyclonal FN1 antibodies (Abcam) were used for WB and IF staining. For the treatment of B16 and D122 cells with IFN-γ, cells 1^{x}10^6 cells were seeded in triplicates and supplemented with recombinant mouse IFN-γ (carrier free) (BioLegend) containing medium (50μg /ml) for 24 hours. For *in vivo* depletion of NK1.1 expressing cells, mice were injected i.p every third day with 25μg of InVivoMAb anti mouse NK1.1, clone PK136 (Bio X Cell). For *in vivo* depletion of CD3 expressing cells, mice were injected every third day with 200μg of InVivoMAb anti mouse CD3ε, clone 145-2C11 (Bio X Cell). For *in vivo* blocking of IFN-γ, mice were injected i.p. every third day with 200μg of InVivoMAb anti-mouse IFN-γ, clone XMG1.2 (Bio X Cell). For recombinant IFN-γ treatment, mice were injected every third day with 100μg of IFN-γ (carrier free) (BioLegend).

CD107a degranulation and cytokine secretion assays

Mice were injected intraperitoneally (i.p.) with 200μg Poly I:C (Sigma Aldrich Israel) and PBLs were harvested 18 hours later. NK cells were isolated using the EasySepT mouse NK cell enrichment kit and co-incubated at 37°C at the indicated ratios, with the target cells in the presence of an APC conjugated anti-mouse CD107a (LAMP-1) (Biotest (121614) for two hours and CD107a levels on the GFP-positive NK cells were determined by flow cytometry. To assess IFN-γ and TNFα secretion, NK cells were isolated from Poly I:C activated PBLs using the EasySepTM mouse NK cell enrichment kit and incubated with B16 cells at 37°C and 5% CO2. Then, supernatants were collected and cytokines levels were measured using standard ELISA.

Evaluation by RCM

In vivo RCM was performed using a reflectance confocal microscope (Vivascope 1500, Caliber I.D. Inc., Rochester, NY, USA). The system uses an 830-nm wavelength diode laser. The laser beam is directed by a dichromatic mirror (beam splitter) toward a pair of mirrors that perform horizontal scanning of the selected skin area. The laser beam then passes through the microscope objective lens

and enters the skin where it can encounter tissue structures of various reflective properties. Next, backscattered light from the tissue re-enters the objective lens and the dichromatic mirror that focuses it onto a gating pinhole. A photomultiplier detector measures the light that enters via the pinhole and produces optical images. The system provides high optical resolution (horizontal axis 2.0μm; vertical axis 5.0μm) to a penetration depth of about 250μm.

Ultrasound gel was used as an immersion medium (refractive index 1.33). A set of sequential horizontal RCM optical sections (each 500um x 500um in area) was acquired at 1.0um intervals from the corneal skin layer (skin surface) to the hypodermis (fatty layer under the skin). For each tumor, we obtained at least 20 images, optically sectioning through the corneal layer, granular and spinous layers, basal layer / epidermal-dermal junction, upper dermis, lower dermis and hypodermis. RCM features of melanoma were recognized and quantified by either counting the number of times they appear in a $1mm^2$ area or by grading them on a 1-10 scale (1 = least aggressive to 10 = most aggressive). Evaluator of the above features was blinded to the genotype of the mice and the tumors.

RCM examination of human melanomas

Figure S1A-R shows two human pigmented skin lesions that appear macroscopically similar, displaying slight asymmetry, minor border irregularities and diameter larger than 0.8cm (S1A and S1J). In routine clinical practice, both lesions would have been surgically removed to rule the possible diagnosis of melanoma. However, RCM evaluation, based on tissue architectural parameters as defined by (Pellacani et al., 2007), enables the differentiation of the two samples into benign nevus (Figure S1A) and malignant melanoma (Figure S1J). The structural parameters tested include 'epidermal disarray', which refers to the disruption of the normal pattern of keratinocytes of the granular and spinous (suprabasal) layers of the epidermis. A nevus (Figure S1B) usually presents regular organization and density of keratinocytes at the suprabasal layers, forming a honeycomb or cobblestone pattern (or a combination of both); in contrast, melanoma (Figure S1K) often displays an irregular pattern of suprabasal epidermal keratinocytes with uneven distribution of the bright cells. Infiltration of the suprabasal epidermis by melanocytes is termed 'pagetoid spread of melanocytes'; the cellular outline of these neoplastic melanocytes can be either dendritic (appearing as bright nucleated cells with branch-like extensions) or round (appearing as round bright nucleated cells with a dark nucleus). Melanocytes in pagetoid pattern infiltrating the suprabasal epidermal layers are commonly seen in melanomas (Figure S1L red arrows) and very rarely in nevi (Figure S1C). 'Pagetoid cellular atypia' in the epidermis is a term that refers to variability in the shape and size of the bright melanocytes; it is another criterion very rarely observed in nevi (Figure S1C), yet noticeable in melanomas (Figure S1L). At the level of the basal layer of the epidermis, normal skin of dark-skin individuals and nevi display a pattern termed 'edged dermal papillae', denoting regular rimming of the dermal papillae by small, bright basal keratinocytes (Figure S1D); the disruption of this normal structure by melanoma creates a pattern termed 'non-edged dermal papillae' (Figure S1M -red circles). At the level of the basal layer of the epidermis, cellular atypia of melanocytes is determined by the presence of large bright cells (at least twice as large as a normal basal keratinocyte), that also show pleomorphism (variability in their size and shape). Cellular atypia of melanocytes is infrequent and relatively minor in nevi (Figure S1E) compared to melanomas (Figure S1N). 'Sheet-like structures' denotes a proliferation of closely-set bright melanocytes within the epidermal-dermal junction, obscuring and eliminating the normal architecture of the junction (that typically includes visible dermal papillae). This phenomenon is observed almost exclusively in melanomas (Figure S1F) and very infrequently in nevi (Figure S1O). While nevi usually exhibit 'homogeneous clusters of melanocytes' (red circles) within the upper dermis (Fig.S1H), 'cerebriform' (Figure S1P) and 'non-homogeneous' (Figure S1Q) aggregates (red circles) appear in melanomas. 'Bright round cells' or 'triangular cells' with well-demarcated dark nucleus (red circle) infiltrate the dermal papilla much more often in melanomas (Figure S1R) than in nevi (Figure S1I). Figure S1S-Z represents the assessment of the RCM criteria in five nevi and eleven confirmed human melanomas. RCM evaluation was performed blindly.

Quantitative PCR (qRT-PCR) and Western Blotting (WB)

mRNA was isolated using R1055 Quick-RNA MiniPrep Kit (Eisenberg bros, Israel) and reversetranscribed to cDNA using M-MLV Reverse Transcriptase 28025-013 (Invitrogen, ThermoFisher Scientific) Quantitative PCR (qRT-PCR) was performed with Platinum® SYBR® Green qPCR SuperMix-UDG w/ROX (ThermoFisher Scientific) in triplicates, normalized to GAPDH and ACTB. For WB, cell lysates were run on 10% SDS-PAGE gel, transferred to a nitrocellulose membrane (Tamar Laboratory Supplies), and stained with GAPDH or Polyclonal FN1 antibody (Abcam, ab2413).

RNA isolation and library construction for transcriptome analysis

Ten to the sixth cells from each of three replicates of B16 or IFN-γ treated B16 cells were lysed and frozen in −80. The libraries were constructed using TrueSeq RNA V2 kit by Illumina.

Processing and Analysis of RNA-Seq Data

Trimming and filtering of raw reads: Raw reads (fastq files) were inspected for quality issues with FastQC (v0.11.2, http://www.bioinformatics.babraham.ac.uk/projects/fastqc/). According to the FastQC report, reads were quality-trimmed at both ends, using in-house Perl scripts, with a quality threshold of 33. In short, the scripts use a sliding window of 5 bases from the read's end and trim one base at a time until the average quality of the window passes the given threshold. Reads that became sorter than 15 bases were discarded.

Mapping and differential expression analysis: The processed fastq files were mapped to the mouse transcriptome and genome using TopHat (v2.0.11). The genome version was GRCm38, with annotations from Ensembl release 76. Mapping allowed

up to 5 mismatches per read, a maximum gap of 5 bases, and a total edit distance of 10 (full command: tophat -G genes.gtf -N 5–read-gap-length 5–read-edit-dist 10–segment-length 20 –coverage-search–read-realign-edit-dist 8–b2-i S,1,0.75–b2-mp 3,1–b2-score-min L,-0.5,-0.5 genome processed.fastq). Quantification, normalization and differential expression were done with the Cufflinks package (v2.2.1). Quantification was done with cuffquant, using the genome bias correction (-b parameter) and the multi-mapped reads assignment algorithm (-u parameter). Normalization was done with cuffnorm (using output format of Cuffdiff) and results were visualized in R, using the cummeRbund package (version 2.8.2) and in-house R scripts. Counts and FPKM distributions, as well as MDS analysis, were used for comparing global expression between samples, outliers evaluation (none were found) and background expression level estimation. Differential expression was calculated with cuffdiff, using a count threshold (-c parameter) of at least 4 for statistical significance testing. Samples were assigned a condition (-L parameter) and the three replicates of INF-treated cells were compared to the three replicates of the non-treated ones. Gene-level cuffdiff output was combined with gene details (such as symbol, Entrez accession, etc.) taken from the results of a BioMart query (Ensembl, release 76). Significantly differentially expressed genes were defined as ones with at least 0.5 FPKM level of expression in at least one of the conditions and a q-value less than 0.05. Differential expression results were visualized in R using the cummeRbund package. Pathway analysis was performed using Ingenuity® Pathway Analysis (IPA®, QIAGEN Redwood City, www.qiagen.com/ingenuity). http://www.illumina.com/products/truseq_rna_sample_prep_kit_v2.html).

Preparation of cryosections and immunofluorescence staining

Tumors were harvested, placed in 30% sucrose solution overnight and then fixed in OCT and frozen in liquid nitrogen. 10 μm slides were cut using Leica CM1950 Clinical Cryostat (Leica Biosystems Nussloch GmbH) and slides were mounted and frozen in −80°C. For immunoflourescent (IF) staining, slides were fixated in methanol at −20°C for 1h, washed twice in PBS and placed in PBS with 1% Triton X-100 (Octyl Phenol Ethoxylate; J.T.Baker). The slides were blocked with CAS-Block Histochemical Reagent 008120 (ThermoFisher Scientific) for 4h at RT. Anti FN1 (Abcam ab2413) was diluted 1:200 in CAS-block and applied to the slides ON at 4°C. Secondary mAb and DAPI were applied following washes with PBS and IF images were captured on an Olympus Fluoview FV1000 confocal microscope 400 or 80 fold magnification. IF staining was performed on tumors harvested from mice, at least five tumors were used in each experiment, and each experiment was repeated at least three times. Representative figures are presented at the indicated magnification. The FV10-ASW version 03.00.01.15 software was used to assess fluorescence intensity.

QUANTIFICATION AND STATISTICAL ANALYSIS

Analysis of Variance (ANOVA) or Student's t test were used to identify significant group differences. To assess survival, the Kaplan Meir model was used followed by the log rank test. $p < 0.05$ was considered significant in all studies, indicated by*. NS; Non-Significant. Details may be found in each figure legend.

DATA AND SOFTWARE AVAILABILITY

Untreated and IFN-γ treated B16 cells RNA seq data are available at the NCBI GEO under accession number GSE106390.

ADDITIONAL RESOURCES

TCGA data analysis was performed using UCSC, Xena, Description: URL: http://xena.ucsc.edu/.